Applied Microbiology and Biotechnology (2024) 108:537
https://doi.org/10.1007/s00253-024-13351-8

BIOTECHNOLOGICALLY RELEVANT ENZYMES AND PROTEINS

TssL2 of T6SS2 is required for mobility, biofilm formation, wrinkly phenotype formation, and virulence of *Vibrio parahaemolyticus* SH112

Xue-rui Bai[1,2] · Peng-xuan Liu[1] · Wen-chao Wang[1] · Ying-hong Jin[3] · Quan Wang[1] · Yu Qi[1] · Xiao-yun Zhang[1] · Wei-dong Sun[4] · Wei-huan Fang[5] · Xian-gan Han[1,6] · Wei Jiang[1]

Received: 3 July 2024 / Revised: 30 October 2024 / Accepted: 4 November 2024 / Published online: 17 December 2024

Abstract

Type VI secretion system 2 (T6SS2) of *Vibrio parahaemolyticus* is required for cell adhesion and autophagy in macrophages; however, other phenotypes conferred by this T6SS have not been thoroughly investigated. We deleted TssL2, a key component of T6SS2 assembly, to explore the role of the T6SS2 in environmental adaptation and virulence. *TssL2* deletion reduced Hcp2 secretion, suggesting that TssL2 played an important role in activity of functional T6SS2. We found that TssL2 was necessary for cell aggregation, wrinkly phenotype formation, and participates in motility and biofilm formation by regulating related genes, suggesting that TssL2 was essential for *V. parahaemolyticus* to adapt changing environments. In addition, this study demonstrated TssL2 significantly affected adhesion, cytotoxicity, bacterial colonization ability, and mortality in mice, even the levels of the proinflammatory cytokines IL-6 and IL-8, suggesting that TssL2 was involved in bacterial virulence and immunity. Proteome analysis revealed that TssL2 significantly affected the expression of 163 proteins related to ABC transporter systems, flagellar assembly, biofilm formation, and multiple microbial metabolism pathways, some of which supported the effect of TssL2 on the different phenotypes of *V. parahaemolyticus*. Among them, the decreased expression of the T3SS1 and T2SS proteins was confirmed by the results of gene transcription, which may be the main reason for the decrease in cytotoxicity. Altogether, these findings further our understanding of T6SS2 components on environmental adaption and virulence during bacterial infection.

Key points

- *The role of T6SS2 in V. parahaemolyticus was far from clear.*
- *TssL2 participates in cell aggregation, wrinkly phenotype formation, motility, and biofilm formation.*
- *TssL2 is essential for cell bacterial colonization, cytotoxicity, virulence, and proinflammatory cytokine production.*

Keywords *Vibrio parahaemolyticus* · T6SS2 · Motility · Biofilm · Wrinkly phenotype · Cytotoxicity

✉ Xian-gan Han
hanxgan@163.com

✉ Wei Jiang
jiangweijw99@163.com

[1] Shanghai Veterinary Research Institute, Chinese Academy of Agricultural Sciences, Shanghai 200241, China

[2] Department of Animal Science and Technology, Shanghai Vocational College of Agriculture and Forestry, Shanghai 201699, China

[3] Institute of Veterinary Medicine, Xinjiang Academy of Animal Sciences, Urumqi 830013, China

[4] College of Veterinary Medicine, Nanjing Agricultural University, Nanjing 210095, China

[5] Institute of Preventive Veterinary Medicine and Zhejiang Provincial Key Laboratory of Preventive Veterinary Medicine, Zhejiang University, Hangzhou 310058, China

[6] Engineering Research Center for the Prevention and Control of Animal Original Zoonosis, Longyan University, Longyan 364012, China

Introduction

Vibrio parahaemolyticus is a causative agent of seafood-borne gastroenteritis worldwide and is a versatile gram-negative bacterium with environmental adaptability and pathogenicity (Han et al. 2019). Hence, a deeper understanding of the mechanisms underlying the pathogenicity and environmental adaptation of *V. parahaemolyticus* is essential for better prevention, diagnosis, and treatment. *V. parahaemolyticus* has a diverse set of virulence factors including hemolysins, proteases, adhesins (Type I pilus), biofilm formation, motility via either polar or lateral flagella, type III secretion systems (T3SSs), and type VI secretion systems (T6SSs) (Ashrafudoulla et al. 2019).

T6SSs are highly conserved and widely distributed among gram-negative bacteria (Singh and Kumari 2023). In some bacteria, they are important for bacterial virulence and environmental adaptation, including biofilm formation, motility, bacterial competition, ion uptake, and cytotoxicity (Coulthurst 2019). *V. parahaemolyticus* RIMD 2210633 possesses genes encoding T6SS1 on VP1386–1420 and T6SS2 on VPA1025–1046 (Zhang et al. 2017a, b). Notably, T6SS1 is mostly associated with clinical isolates of *V. parahaemolyticus*, while T6SS2 is found in all analyzed strains (Ronholm et al. 2016; Yu et al. 2012). The genome sequence of a serotype O3:K6 *V. parahaemolyticus* SH112 strain also revealed the presence of two putative type VI secretion systems (T6SSs), based on previous genetic comparisons with *V. parahaemolyticus* RIMD 2210633. When multiple T6SS gene clusters are found in a single bacterial genome, the different systems typically possess different functions and regulatory mechanisms (Wang et al. 2013). The two T6SSs in *V. parahaemolyticus* are differentially regulated by environmental signals such as quorum sensing, temperature, salinity, and osmolarity (Salomon et al. 2013; Huang et al. 2017). The VpT6SS2 genes are expressed and the system fires under low salt media (containing 1% sodium chloride) and temperature (23 ~ 30 °C) conditions (Salomon et al. 2013), similar to those observed with *Vibrio fluvialis* T6SS2 (Pan et al. 2018). In addition, VpT6SS2 regulates adhesion to host cells and autophagy of macrophage cells but not cytotoxicity, the latter of which is different from VpT6SS1 (Yu et al. 2012; 2015). However, other roles of VpT6SS2 have not been reported.

The T6SS device is assembled from 14 well-conserved core components (TssA-M, PAAR), which are divided into four macromolecular structures, namely baseplate complex, membrane complex, contractile structure, and puncturing device (Reglinski et al. 2023). This apparatus anchors to cell membranes by membrane complex (TssJLM), then recruits baseplate complex (TssEFGK), and under the contracting action of contractile sheath (TssBC), drives the puncturing device (comprising Hcp, VgrG/PAAR) into an adjacent target cell for cell killing (Reglinski et al. 2023). Among them, Hcp secretion is often used as the hallmark of functional T6SS (Singh and Kumari 2023, Yu et al. 2012). TssL (DotU), as a component of the membrane complex, plays a central role for T6SS assembly and Hcp secretion (Wang et al. 2018a, b). In addition, in the avian pathogenic *Escherichia coli* (APEC), TssL plays key roles in pathogenesis and intracellular host response modulation (Wang et al. 2014). In *Francisella tularensis*, TssL is essential for maintaining the intracellular lifecycle and virulence (Bröms et al. 2012). Moreover, TssL is critical to the biofilm formation, pathogenicity, and invasiveness in *Aeromonas veronii* (Song et al. 2020). Understanding whether TssL2 of T6SS2 has similar functions may provide insights into the role of *V. parahaemolyticus* in environmental adaptation and pathogenicity.

In this study, we used homologous recombination to delete *tssL2* (*vpA1040*) from *V. parahaemolyticus* SH112 strain, producing the deletion mutant *ΔtssL2* and its complemented strain. We analyzed the differences in biofilm formation, colony morphology, motility, flagellar formation, bacterial competition, cytotoxicity, colonization, mouse mortality, and expression of macrophage cytokines between the mutant, complementary, and wild-type (WT) strains.

Materials and methods

Bacterial strains, reagents, plasmids, and growth conditions

The microbiological media used in this study were purchased from Oxoid Ltd (Basingstoke, Hampshire, England) and Sangon Biotech (Shanghai, China); the reagents and antibiotics were purchased from Sigma-Aldrich (St. Louis, MO, USA). The *V. parahaemolyticus* SH112 strain (GenBank: JACYGZ000000000.1) was isolated from a clinical specimen in Shanghai and stocked in the China General Microbiological Culture Collection Center under the accession number CGMCC 1.90013 and was used as the WT strain (Li et al. 2022). The *V. parahaemolyticus* strains in this study were cultured in Luria–Bertani (LB) broth supplemented with 2% sodium chloride at 30 °C, with shaking at 160 rpm (Noh et al. 2015). *V. parahaemolyticus* was identified using Thiosulfate-citrate-bile salts-sucrose agar culture medium (TCBS Agar; HKM, Guangdong, China). For gene cloning and the construction of gene deletion mutants, *Escherichia coli* CC118 λpir was grown in LB medium at 37 °C (Li et al. 2022). The suicide plasmid pYAK1 and the plasmid pMMB207 were used to generate gene deletion

mutants and complemented strains (Li et al. 2022). The WT and derivative strains of *V. parahaemolyticus* and *E. coli* are listed in Table S1 of the supplemental material. Antibiotics were administered at the following concentrations: 10 μg/mL chloramphenicol and 70 μg/mL kanamycin.

Bacterial concentrations in LB medium were estimated using 96-well microtiter plates (100 μL) based on absorbance OD_{600} (optical density at 600 nm) values recorded with a microplate spectrophotometer (Multiskan GO, Thermo Fisher Scientific, Waltham, MA, USA), or using the standard plate count method with incubation at 30 °C for 16 h in LB medium containing 1.5% agar.

For swimming motility and transmission electron microscopy (TEM) assays, culture plates containing LB medium with 0.3% agar (0.3% agar-LB plates) were incubated at 30 °C overnight. For swarming motility assays, heart infusion (HI) medium plates containing 1.5% agar (1.5% agar-HI plates) were used. For colony morphology assays, LB medium plates containing 2% agar (2% agar-LB plates) and Congo red (CR) plates were used. The CR plates were prepared using 2% agar-LB after autoclaving and then by adding 40 μg/mL filtered Congo red and 20 μg/mL Coomassie brilliant blue R (Yuanye Bio-Technology, Shanghai, China).

Construction of deletion mutants

We followed previously published methods (Yu et al. 2012; 2015) to generate the *vpA1040* deletion mutant strain. Briefly, two DNA fragments were amplified by PCR, using WT DNA as the template and the primer pair *tssL2*-A/B or *tssL2*-C/D, respectively (Table S2 in the supplemental material). Next, the *tssL2*-AB (425 bp upstream of the start codon) and *tssL2*-CD (487 bp upstream of the stop codon) fragments were used as the templates with the primers *tssL2*-A/D to construct a *tssL2* deletion fragment via PCR amplification. After recovery and purification using agarose gel, the deletion fragment was digested with restriction enzymes *BamH*I and *Sph*I, ligated into pYAK, and then digested with the same restriction enzymes to produce pYAK-*tssL2*-AD. This plasmid was transformed into *E. coli* CC118 λpir to obtain the strain pYAK-*tssL2*-CC118 λpir, which was then conjugated into the *V. parahaemolyticus* SH112 WT strain. TCBS agar plates supplemented with chloramphenicol (10 μg/mL) and LB agar plates containing 20% sucrose were used to screen the *V. parahaemolyticus* cells with the gene deletion from one generation to another until clones were unable to grow on the TCBS plates. After continuous culturing, suspected positive clones were isolated, cultured in LB, and confirmed by PCR with *tssL2*-E/F primers (deletion mutants, 1222 bp). Meanwhile, *sacB*-E/F primers (deletion mutants, 500 bp) were used to confirm whether the deletion mutant had discarded the pYAK plasmid. After further confirmation by sequencing, positive colonies were designated as the Δ*tssL2* strain.

Construction of complementary strains

The entire open reading frame fragment of *tssL2* (1538 bp) was amplified by PCR with *V. parahaemolyticus* SH112 DNA as the template and *tssL2*-pMMB-F/R primers (Table S2 in the supplemental material). After digestion with restriction enzymes *EcoR*I and *BamH*I, the sequence was ligated to the digested pMMB plasmid to obtain the plasmid *tssL2*-pMMB. This plasmid was transformed into and propagated in *E. coli* CC118 λpir. Then, *tssL2*-pMMB-CC118 λpir was conjugated to Δ*tssL2*, which further developed into a complementary strain through several generations under chloramphenicol selection. The positive complementary strains were identified using PCR with *tssL2*-pMMB-F/R primers and were ultimately designated as CΔ*tssL2*.

Sequence analysis of tssL2 gene and TssL2 protein

The nucleotide sequences of *tssL2* gene from other *V. parahaemolyticus* strains and representative *vibro* spp. were downloaded from NCBI and aligned with the sequence of TssL2 in this study using Mesquite software (Zhang et al. 2020). In addition, the TssL2 protein structure of *Vibrio paraholyticus* was analyzed by protein structure online prediction website (Song et al. 2020).

Extraction of mRNA and qRT-PCR

QRT-PCR was used to assess the transcriptional level of corresponding mRNAs in *V. parahaemolyticus* strains and infected cells, as reported previously (Yu et al. 2012). Total RNA was isolated from centrifuged bacteria or collected cells using the TRizol® reagent (Invitrogen, Carlsbad, CA, USA). Residual DNA digestion and cDNA preparation were performed using a Prime Script® RT reagent Kit with gDNA Eraser (RR047A, Takara Bio, Shiga, Japan) according to the manufacturer's protocol. Real-time PCR was performed on the Applied Biosystems® 7500 Fast Real-time PCR system (4,406,985, Applied Biosystems, Waltham, MA, USA) using SYBR® *Premix Ex*Taq™ II (RR820A, Takara Bio, Shiga, Japan) and designed gene-specific primers (see Table S3 in the supplemental material) in a reaction mixture with a total volume of 20 μL. The PCR thermocycling protocol comprised 30 cycles of 94 °C for 15 s, 54 °C for 30 s, and 68 °C for 1 min. Using the comparative cycle threshold ($2^{-\Delta\Delta CT}$) method (Wang et al. 2016), relative gene expression was normalized to the expression of the housekeeping gene *gap* in *V. parahaemolyticus*. Experiments were repeated with three biological and three technical replicates.

Analysis of transcription, expression and secretion of T6SS2

For analysis of T6SS2 transcription, the genes *vgrG2* (*vpA1026*), *hcp2* (*vpA1027*), *tssM2* (*vpA1039*), *tssL2* (*vpA1040*), *tssK2* (*vpA1041*), *vpA1044* were selected for detection using qRT-PCR (see Table S3 in the supplemental material). Three strains (WT, Δ*tssL2*, and CΔ*tssL2*) were harvested in LB medium and then grown until reaching the logarithmic growth phase ($OD_{600}=0.2$), and extraction of mRNA and qRT-PCR were performed.

For analysis of T6SS2 expression and secretion, Hcp2 was selected for detection using Western blot (Salomon et al. 2013). High-density *V. parahaemolyticus* strains were acquired by culturing in LB medium at 28 °C for 4 h. The strains were then cultured in Dulbecco's modified Eagle's medium (DMEM, Gibco®, Grand Island, NY, USA) with low-glucose and low-salt conditions for 6 h at 28 °C and centrifuged at 5000 × *g* for 30 min. The secreted supernatant proteins and pellet proteins were collected and separated using 12% sodium dodecyl sulfate–polyacrylamide gels. The proteins were transferred onto polyvinylidene difluoride (PVDF) membranes (Amersham Biosciences, Amersham, UK) using the Trans-Blot® SD semi-dry transfer cell (Bio-Rad, USA). Rabbit anti-thermostable direct hemolysin (TDH) antibody and anti-cytosolic marker AMP receptor protein (Crp) antibody were used as a positive and lysis control, and anti-Hcp2 polyclonal antibodies were used to specifically bind to secreted proteins, which were then detected with goat anti-rabbit IgG-HRP (Sigma-Aldrich, St. Louis, MO, USA).

Bacterial killing assays

As previously described (Salomon et al. 2014), *V. parahaemolyticus* strains were incubated overnight, subcultured in fresh LB medium and then grown until reaching the logarithmic phase ($OD_{600}=0.2$). After washing and resuspending in 1 × phosphate-buffered saline (PBS), the three *V. parahaemolyticus* strains were mixed with *E. coli* DH5α in a 4:1 ratio and analyzed in triplicate. Next, the bacterial mixture was split into two samples; one was incubated at 30 °C for 4 h, and the other was used to spot tenfold serial dilutions on LB and LB plus ampicillin plates to determine initial concentrations of *E. coli* and *V. parahaemolyticus*. The *V. parahaemolyticus* strains used in this study were resistant to ampicillin, as recently reported (Mala et al. 2016), but DH5α was not. After 4 h, incubated suspensions were cultured on LB and LB with ampicillin plates to confirm the bacterial survival rate; these assays were repeated three times.

Aggregation assay

As reported previously (Levinson et al. 2015; Liu et al. 2012), overnight cultures of all strains were diluted to 1:100 with 5 mL of LB medium in glass test tubes and grown to equal OD_{600} values (approximately 0.25). All the tubes were shaken vigorously for 15 s before the start of the assay and were then statically cultured at 22–24 °C for 72 h. Four replicates were prepared for each strain. One of the tubes was used to photograph the culture suspension, and the other three replicates were used to regularly confirm OD_{600} values of 100 µL samples from the liquid surface to determine aggregation. The experiment was performed independently in triplicate.

Evaluation of bacterial biofilms

Following a published crystal violet staining method (Kimbrough et al. 2020), *V. parahaemolyticus* strains were subcultured into fresh LB and grown to the logarithmic phase ($OD_{600}=0.2$) by shaking at 30 °C for 6 h. The strains were diluted to 1:100 in 5 mL LB in glass test tubes and were grown at room temperature with no shaking for 72 h. Biofilms at the air–liquid interface were visualized and imaged. Notably, as the newly formed biofilm was highly vulnerable to destruction, the tube should not be moved during the process of biofilm formation, and extra care must be taken when moving the tube for imaging. Then, cultures were carefully decanted to acquire the biofilm and associated cells adhering to the walls of the tube. After the biofilm was air-dried, it was stained with 5 mL of 1% Crystal Violet for 30 min at 22–24 °C and then thoroughly washed with 1 × PBS. Finally, the adherent biofilm was solubilized using 5 mL of 100% ethanol for 10 min, then the absorbance was measured at 600 nm. The experiment was performed at least three times.

In addition, qRT-PCR for biofilm-related regulatory genes (*calR*, *cspQ*, *mfpA*, *aphA*, *opaR*, *luxS*, *mshA*, *oxyR*, *cspA*) in *V. parahaemolyticus* SH112 were performed (Faleye et al. 2021). For qRT-PCR, the strains were grown in 2.5% (w/v) HI broth (ELITE Biotech, Shanghai, China) at 37 °C shaking at 250 rpm. Briefly, overnight cultures were 50-fold diluted in 15 mL of fresh HI broth, and harvested at the mid-exponential growth phase ($OD_{600}=0.5$). Subsequently, resulting cultures were diluted 1000-fold into 15 mL of fresh HI broth for a third round of cultivation, and extraction of mRNA were performed as described above. When necessary, 50 µg/mL gentamicin was supplemented in the medium.

Colony morphology

The colony morphology assays were performed as described (Kimbrough et al. 2020; Martín-Rodríguez et al. 2021), with modifications. Briefly, the strains were statically cultured in

LB medium until reaching the logarithmic growth period. Next, 2.5 µL samples of the resultant culture were inoculated on 2% agar-LB plates and CR plates and incubated at 30 °C for 48 h before culturing for 5 days at 22–24 °C. All colony morphology images were obtained on day 6.

Motility assay

As described previously (Guo et al. 2019), the strains were freshly grown in LB broth with 2% sodium chloride at 30 °C until they reached equal optical densities ($OD_{600}=0.2$). To observe swimming motility, 2 µL of each culture sample was inoculated on the surface of 0.3% agar-LB plates with 2% sodium chloride and incubated for 4 h at 30 °C. For the swarming assay, cultures were performed similarly to the swimming assays but on 1.5% agar-HI plates for 24 h at 30 °C. For both motility assays, the diameters of the bacterial motility halos were measured and recorded.

Observation and gene transcription assays of flagella

The ultrastructures of the flagella of the WT and Δ*tssL2* strains were observed through high-resolution TEM (FEI, Ltd., Hillsboro, OR, USA) using the negative staining method with phosphotungstic acid to examine correlation of morphological factors with motility (Li et al. 2022). The strains were separately inoculated on 0.3% agar-LB plates with 2% sodium chloride and incubated for 4 h at 30 °C to observe bacterial polar flagella (Noh et al. 2015). Single colonies of each strain were then gently suspended in 1 × PBS and negatively stained with 2% phosphotungstic acid (Sigma-Aldrich, St. Louis, MO, USA). The stained bacteria were adhered to grids, air-dried, and observed with TEM. The ratios of damaged and fractured polar flagella (including surrounding or scattering attached flagella) in three strains were calculated as the number of the polar flagella damaged and fractured/the total number of the polar flagella × 100%. To validate the TEM results, qRT-PCR was used to measure the transcription levels of the flagellar protein-associated genes of *V. parahaemolyticus* on chromosomes I and II in polar and lateral flagella (Masum et al. 2017; Noh et al. 2015). To obtain swimming- and swarming-related mRNAs, the strains were assembled on 0.3% agar-LB plates with 2% sodium chloride for 4 h post-incubation and on 1.5% agar-HI plates for 24 h. The structural polar flagellar (*flaA*, *flgE*, *flgM*, *fliD*, *fliF*, *fliG*, *motB*) and lateral flagellar (*lafA*, *flgB*, *flgM*, *fliD*, *fliE*, *fliM*, *motB*, *motY*) genes were selected for detection using qRT-PCR (see Table S3 in the supplemental material). The experiments were repeated in triplicate, with four replicates per strain.

Adhesion and cytotoxicity assay

Adherence and cytotoxicity tests of *V. parahaemolyticus* strains on Caco-2 cell monolayers were performed using as previously described (Yu et al. 2012; Ming and Sheng 2015). Briefly, Caco-2 cells were grown in DMEM supplemented with 20% FBS without antibiotics. For adherence assay, monolayer cells (approximately 5×10^5 cells per well in 24-well cell plates) were co-cultured with PBS-washed bacteria in DMEM at a multiplicity of infection (MOI) of 1:10, and incubated at 37 °C for 1 h. After washed twice with 1 × PBS, the cells completely lysed with 0.5% Triton X®-100. Subsequently, serial tenfold dilutions of bacteria-containing lysates were plated onto LB agar plates, and the number of single colonies of each strain was recorded. Percent adherence was expressed as bacterial cells adhered/bacterial cells added into the well × 100.

For cytotoxicity assay, Caco-2 cells were cultured in a 96-well plate (approximately 2×10^4 cells per well). Before infection, the cell monolayers were washed with 1 × PBS and were inoculated with three strains at an MOI of 1:10 in DMEM, then respectively incubated at 37 °C for 0.5, 1, 1.5, 2, 2.5, 3 h. The culture supernatants containing lactate dehydrogenase (LDH) were collected according to the manufacturer's instructions for the CytoTox 96® Non-Radioactive Cytotoxicity Assay Kit (Promega, Madison, WI, USA). The spontaneous (positive) and maximum (control) release of LDH was measured from the cytoplasm of uninfected Caco-2 cells without or with the addition of 0.8% Triton X-100, respectively. Sample absorbance values (OD_{490}) were measured using a microplate reader and expressed as the percentage of the positive and control values. Percentage cytotoxicity was calculated using the formula: (test LDH release − spontaneous release)/maximal release.

Acute toxicity studies in mice

As previously described (Flood and Kondo 2004), acute toxicity testing was performed on 4-week-old, specific-pathogen-free ICR (Institute of Cancer Research) mice purchased from the Slack Shanghai Laboratory Animal Co., Ltd. (Shanghai, China). The mice were randomly assigned to 15 treatment groups, each containing eight mice. When growth reached the logarithmic phase ($OD_{600}=0.2$), bacterial suspensions were adjusted to 200 µL doses per mouse of 4×10^7, 2×10^7, 1×10^7, 5×10^6, and 2.5×10^6 CFU. The mice were injected intraperitoneally with different bacterial concentrations for the three strains. In addition, five mice were inoculated with sterile physiological saline as the control. The animals were observed for 7 days, and 50% lethal dose (LD_{50}) was calculated using the Reed–Muench method (Yi et al. 2013).

Infection experiments in mice

After confirming the LD_{50} of an intermediate dose (1.5×10^7 CFU per animal), four groups containing twelve 4-week-old ICR mice each received an intraperitoneal injection of bacteria (WT, Δ*tssL2*, or CΔ*tssL2*) or sterile physiological saline. Survival was monitored once every 5 h until 7 days post-infection. Three mice were selected from each group at 20 h post-infection to assess the presence of viable bacteria in infected organs. Blood samples were drawn by ocular enucleation, and an anticoagulant (sodium citrate) was added. After aseptic anatomical sampling, tissue (0.2 g and 0.1 g from the liver and spleen, respectively) and blood samples (100 µL) were homogenized, diluted tenfold in sterile physiological saline, and plated onto TCBS agar to evaluate bacterial colonization. By counting the bacterial colonies on the plates, the degree of bacterial colonization in the blood, liver, and spleen of ICR mice was calculated.

Cytokine assays

Caco-2 cells in 24-well plates were infected with the three strains at an MOI of 1:100, with uninfected Caco-2 cells in the medium serving as the control group. After infection with the *V. parahaemolyticus* strains for 1 h, monolayer Caco-2 cells were treated with gentamicin (200 µg/mL), then washed three times with 1 × PBS. After culturing for 1, 2, 3, and 4 h, Caco-2 cells were collected, and total mRNA was extracted for RT-PCR (Zhou et al. 2013a, b). The primer sequences for interleukin-6 (IL-6), IL-8, and β-actin (as an internal control) are listed in supplemental material Table S3.

Sample preparation and label-free quantitative mass spectrometry

Three biological replicates of the WT and Δ*tssL2* strains (WT-1, WT-2, WT-3 and Δ*tssL2*-1, Δ*tssL2*-2, Δ*tssL2*-3) were grown in 50 mL DMEM media at 28 °C with vigorous agitation for 6 h, and centrifuged at 5000 × *g* for 30 min at 4 °C. The secretory proteins in the culture supernatant were prepared using a customized procedure by label-free quantitative mass spectrometry (APTBIO, Shanghai, China). Briefly, secretory proteins in 40 mL of culture supernatant were freeze-dried by liquid helium and cleaved with 1 mL SDT (%[w/v] SDS, 100 mM Tris/HCl pH 7.6, 0.1 M DTT), then quantified using the BCA protein assay. Collected proteomes were lysed with trypsin to complex peptide mixtures by filter-aided sample preparation, and then the peptides were desalted by C_{18} cartridge. Each sample was separated by high performance liquid chromatography using the EASY-nLC1200 system, and the separated peptides were eluted with water containing 0.1% formic acid (FA) and 84% acetonitrile containing 0.1% FA at a flow rate of 300 nL min^{-1}. Peptide analysis was performed with Q-exactive mass spectrometer, and the differentially expressed proteins (DEPs) were subjected to bioinformatics analysis in accordance with the criteria of p value of < 0.05 and fold changes > 2.0 or < 0.5. GO and KEGG enrichment analyses based on Fisher's exact test were performed.

Gene transcription assays of T3SS1 and T2SS

QRT-PCR was used to measure the transcription levels of T3SS1 and T2SS genes of *V. parahaemolyticus* (Lian et al. 2022). To obtain mRNAs, the strains were cultured in LB medium at 37 °C until they reached the logarithmic phase ($OD_{600} = 0.2$). The T3SS1 (*vopD*, *vopB*, *vscP*, *vecA*, *vopR*, *vopS*, *vscJ*, *vscG*) and T2SS (*gspC*, *gspE*, *gspJ*, *gspL*, *gspM*) genes were selected for detection using qRT-PCR (see Table S3 in the supplemental material).

Statistical analysis

The TEM observations were repeated twice, and other assays were repeated thrice, each with least three replicates per strain. Data were displayed as mean ± standard deviation (SD) and analyzed in Graph Pad Prism (v5; Systat Software Inc., Chicago, IL, USA). Differences were considered significant when $P < 0.05$, as denoted by one asterisk (*); outstanding significance was achieved when $P < 0.01$, as denoted by two asterisks (**); and extremely remarkable significance was achieved when $P < 0.001$, as denoted by three asterisks (***).

Results

Sequence characterization of TssL2

V. parahaemolyticus has a complete T6SS2 genome, including *vgrG2* (*vpA1026*), *hcp2* (*vpA1027*), *tssM2* (*vpA1039*), *tssL2* (*vpA1040*), *tssK2* (*vpA1041*), *vipA2* (*vpA1035*), *vipB2* (*vpA1034*) (Ma et al. 2012). The total length of *tssL2* gene of *V. parahaemolyticus* SH112 strain was 1293 bp, and the sequence characterization of TssL2 revealed approximately from 97.8 to 100% overall sequence identity with the DotU family T6SS2 proteins of other *V. parahaemolyticus* strains and 73.2%, 69.9%, 56.4%, with other *Vibrio* strains *V. antiquarius* (NC_013457.1), *V. harveyi* (NZ_CP125876), *V. vulnificus* (NZ_CP012882), respectively. TssL2 protein contains 430 amino acids and has a molecular weight of ~ 75 kDa. The primary structure of TssL2 protein contains transmembrane structure and does not contain signal peptide. The secondary structure analysis showed that TssL2 protein consisted of 46.05% α helix, 47.67% random coil, and 6.28% extended

chain, which were mainly composed of α helix. In addition, TssL2 protein encodes DotU and C-terminal OmpA-like domains, the latter being ligand binding sites. Homology analysis showed that TssL2 had 82%, 29%, 26%, 25% homology with an unknown protein (D0XF19.1.A), TssL2 from *V. cholerae*, putative OmpA-family membrane protein from *Yersinia pestis*, and T6SS TssL/SciP from *E. coli* (see Fig. S1 in the supplemental material).

TssL2 is required for T6SS2 functional integrity

The *tssL2* mutant and complemented strains were successfully constructed, showing no significant differences from the WT strain in bacterial growth on LB or HI medium (see Fig. S2 in the supplemental material). The VpT6SS2 genetic region is composed of three operons, VPA1027-1024, VPA1044-1028, and VPA1044-1046 (Zhang et al. 2017a, b). To test whether TssL2 affects gene transcription of important components of VpT6SS2, qRT-PCR assays were performed. The result showed that transcription levels of T6SS2 genes (*vpA1026*, *vpA1027*, *vpA1039*, *vpA1041*, *vpA1044*) in Δ*tssL2* were not significantly different compared to WT (Fig. 1A). Therefore, *tssL2* deletion had no significant effect on expression of the *vgrG*, *hcp2*, *tssM2*, or other upstream and downstream genes in the T6SS2 locus of *V. parahaemolyticus* SH112. Meanwhile, *tssL2* (*vpA1040*) was not detected on the mutant strain and the expression was restored in the complemented strain, suggesting that TssL2 of Δ*tssL2* strain was inactivated and that of CΔ*tssL2* strain was restored.

To test whether T6SS activities are affected in Δ*tssL2*, the levels of Hcp2 (VPA1027) production and secretion were detected by Western blot. With TDH and Crp used as positive controls, Hcp2 was detected in the cell pellets of WT, Δ*tssL2* and the complemented strain CΔ*tssL2*, and the culture supernatants of WT and CΔ*tssL2* (Fig. 1B). Reduced levels of Hcp2 protein were detected in the supernatant and cell pellets of the Δ*tssL2* strain, indicating that TssL2 was necessary for Hcp2 secretion in *V. parahaemolyticus* SH112.

TssL2 is required for T6SS2-mediated antibacterial ability

The T6SS2 of *V. fluvialis* confers antibacterial activity to the strain (Pan et al. 2018). To investigate whether T6SS2 affects antibacterial ability, we performed bacterial killing assays by employing *E. coli* DH5α as prey. Under similar conditions, *E. coli* incubated with Δ*tssL2* showed significantly higher survival than that incubated with WT. Meanwhile, there was no significant difference in the survival of attacker strains (Fig. 1C). Altogether, these results indicated that TssL2 of T6SS2 contributed to the competition ability of *V. parahaemolyticus* SH112.

TssL2 weakens biofilm and wrinkly phenotype formation

To investigate whether the absence of *tssL2* affects biofilm formation, we compared the differences in biofilm formation between the three strains (WT, Δ*tssL2*, and CΔ*tssL2*). The Δ*tssL2* mutant had visibly thicker biofilm-like aggregates on the liquid surface and more transparent culture medium, compared to WT and CΔ*tssL2* (Fig. 2A). The differences in biofilm formation of the strains were quantified by the crystal violet staining assay, showing that Δ*tssL2* exhibited increased biofilm formation with values 3.2-fold higher than those of WT, and CΔ*tssL2* exhibited similar biofilm production to that of WT (Fig. 2B). To further examine whether the culture medium containing Δ*tssL2* was related to cell aggregation, OD_{600} values of the three strains in the sub-surface liquid were evaluated. Aggregation assays showed that the OD_{600} values of Δ*tssL2* were significantly lower than those of the WT strain at 72 h (Fig. 2C). Interestingly, the OD_{600} value of Δ*tssL2* was almost constant, whereas that of WT strain showed an elevated S-curve pattern. These results indicated that TssL2 weakens biofilm formation and cell aggregation in *V. parahaemolyticus* SH112. QRT-PCR analysis showed that the biofilm-related genes *calR*, *cpsQ*, *mfpA*, *aphA* showed markedly higher transcription, and *opaR* showed lower transcription in Δ*tssL2* than in WT (Fig. 2D). Meanwhile, although the expression of these genes did not differ between the CΔ*tssL2* and WT strains, the *cpsQ* and *aphA* transcription in CΔ*tssL2* strain were 0.47-fold and 0.44-fold higher than the wild strain. These results suggested that TssL2 affected biofilm-related gene expression levels and therefore led to aberrant biofilm formation.

Colony morphology is closely related to the synthesis of exopolysaccharides, which form an important component of biofilms. Therefore, we next examined whether TssL2 could influence bacterial colony morphology using Congo red staining. In LB (Fig. 2E) and CR plates (Fig. 2F), Δ*tssL2* formed rugose and marginally transparent colonies (wrinkly phenotype), whereas the WT strain produced completely smooth and opaque colonies (smooth phenotype). The complemented strain showed atypical colony morphology between wrinkly and smooth phenotypes, indicating that CΔ*tssL2* partly restored to the level of WT strain, maybe due to the reason that the plasmid-borne TssL2 could only partly increased the phenotypes in CΔ*tssL2*. These results suggested that TssL2 weakened smooth-wrinkly phenotype switching.

TssL2 is required for lateral flagella- and polar flagellum-mediated motility

To determine whether TssL2 impacts motility, we performed swimming and swarming assays. Swimming assays showed that the WT strain produced a large, pellucid, dentate, diffuse halo, whereas Δ*tssL2* was non-motile, and the complemented

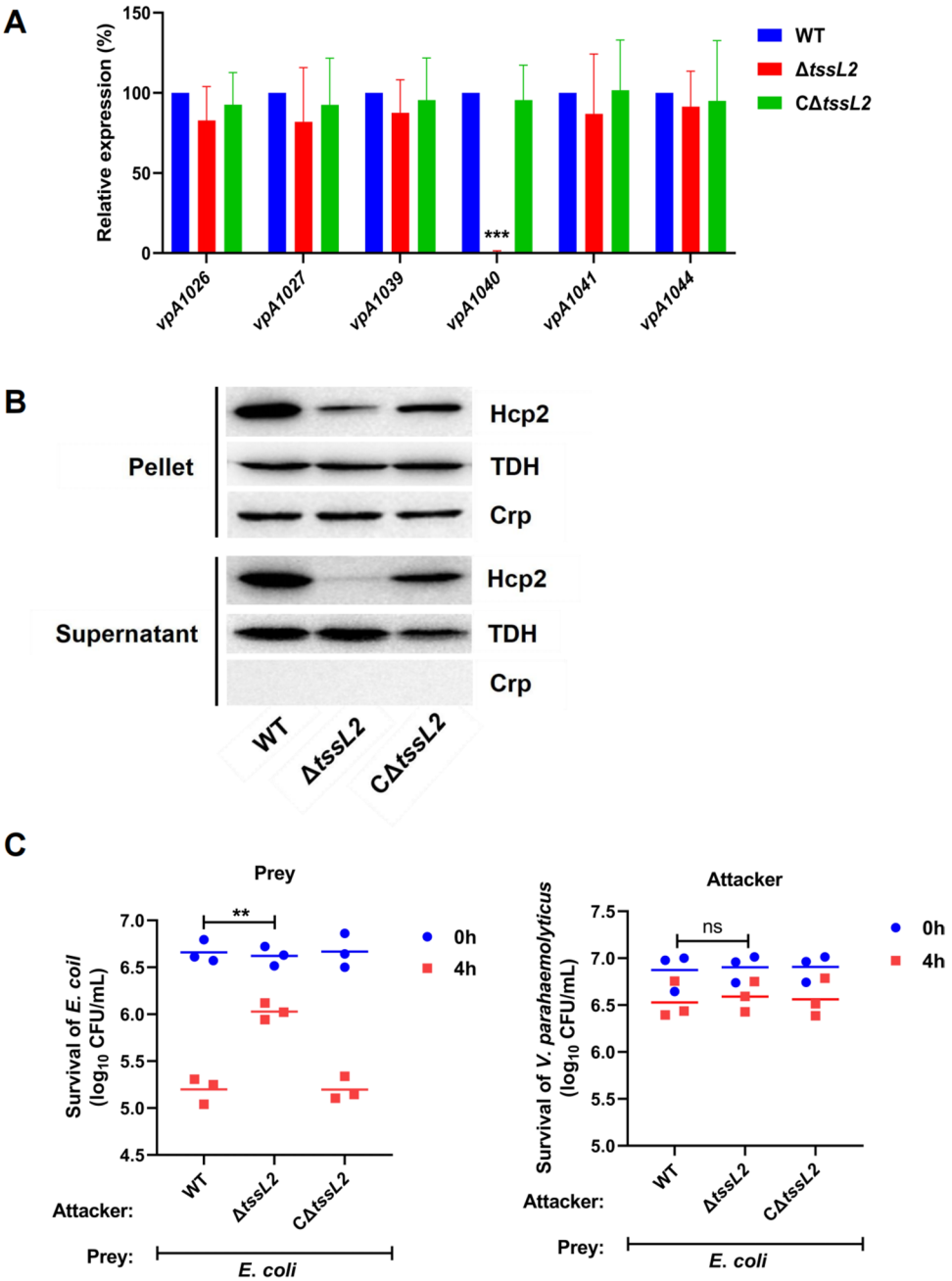

Fig. 1 Mutation in *tssL2* influences Hcp2 expression and VpT6SS2-dependent antibacterial activity. **A** The relative mRNA levels of VpT6SS2 genes were compared between WT, Δ*tssL2*, CΔ*tssL2* strains. Data are shown as mean ± SD ($n = 4$) of 2 independent experiments with 2 replicates, using two-way ANOVA (***$P < 0.001$). **B** Analysis of Hcp2 expression in pellets and supernatants of WT, Δ*tssL2*, CΔ*tssL2* strains with Hcp2 polyclonal antibodies using western blotting to assess T6SS2-related Hcp2 secretion; TDH and Crp production were used as a positive and lysis control. **C** A bacterial killing assay was performed between *Vibrio parahaemolyticus* (attacker) and *Escherichia coli* (prey) at a 4:1 OD_{600} ratio (attacker:prey). Viability counts of *E. coli* and *Vibrio parahaemolyticus* were determined at 0 h and 4 h after co-culture. Statistical significance between strains at 0 h and 4 h timepoint was assessed using two-way ANOVA test (**$P < 0.01$; *ns*, not significant)

strain restored swimming ability. Based on the motility halo diameter (cm), the swimming motility of Δ*tssL2* was lower than that of WT (Fig. 3A). The swarming assay showed that *tssL2* deletion significantly attenuated swarming motility compared to that in WT. The complemented strain partly restored the swarming ability of WT, maybe due to the reason that the plasmid-borne TssL2 could only partly increased the phenotypes in CΔ*tssL2* (Fig. 3B). These results indicated that the inactivation of TssL2 in T6SS2 contributed to swimming and swarming motility of *V. parahaemolyticus* SH112.

To demonstrate the role of TssL2 in flagellum formation, we firstly observed the morphology of flagella in Δ*tssL2* and WT cells via TEM and found that the lateral flagella of Δ*tssL2* cells were absent, compared to WT and CΔ*tssL2* (Fig. 3C). Moreover, the ratio of damaged and fractured polar flagella in Δ*tssL2* strain (91.6%) was significantly higher than that in WT (26.9%) and in CΔ*tssL2* (38.8%). The Δ*tssL2* strain was more likely to produce damaged and fractured polar flagella; in contrast, the WT and CΔ*tssL2* strains exhibited long polar flagella (Fig. 3D). According to these results, the Δ*tssL2* strain had a high probability of producing impaired polar flagella, which could explain the decreased swimming motility. This strain also exhibited a high probability of delayed

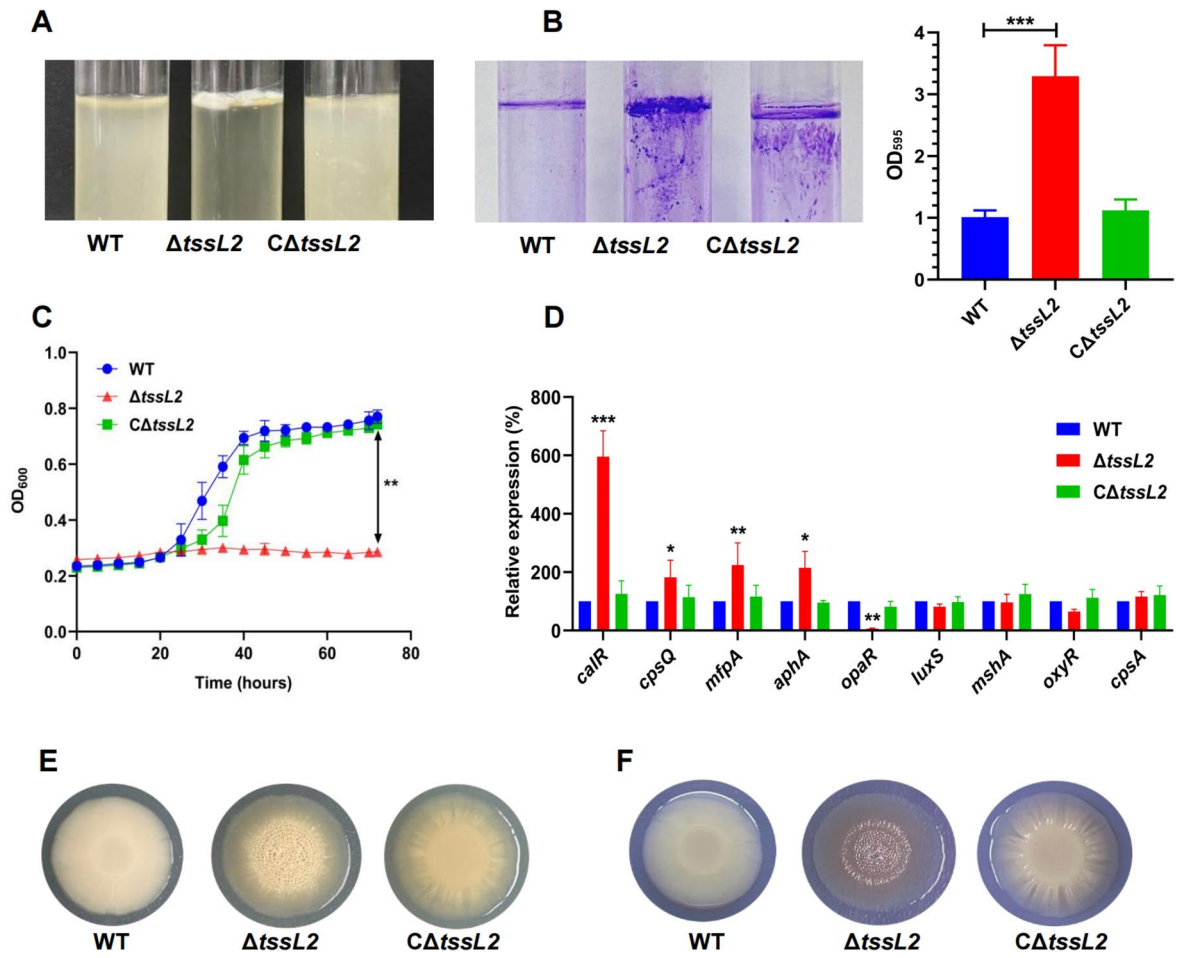

Fig. 2 *TssL2* deletion aids in biofilm formation, bacterial aggregation, and wrinkly phenotype formation. **A** In LB medium, biofilms and liquid suspensions of the WT, Δ*tssL2*, and CΔ*tssL2* strains were observed visually after 72 h. **B** Crystal violet staining was performed to quantify biofilm, and OD_{595} values were analyzed by one-way ANOVA. **C** OD_{600} values of three strains in the sub-surface liquid were applied to quantitatively evaluate bacterial aggregation. Asterisk denotes statistical significance between WT and Δ*tssL2* strain at 72 h by two-way ANOVA test (***$P<0.001$). **D** QRT-PCR for the expression of biofilm-related genes (*calR*, *cspQ*, *mfpA*, *aphA*, *opaR*, *luxS*, *mshA*, *oxyR*, *cspA*) in *V. parahaemolyticus*. Data are shown as mean ± SD ($n=4$) of 2 independent experiments with 2 replicates, using two-way ANOVA, and asterisks denote statistical significance between WT and Δ*tssL2* strains (*$P<0.05$; **$P<0.01$; ***$P<0.001$). With 2% agar, LB plates (**E**) and LB plates containing CR plates (**F**) showing bacterial colony morphology after 72 h

and/or constrained growth of lateral flagella, thereby weakening swarming motility.

As motility is dependent to the regulation and assembly of bacterial flagella, we explored the expression of several flagellar biogenesis genes in Δ*tssL2*. Our assays showed that the expression of the polar flagellar genes (*flgE*, *fliF*, *fliG*, *flaA*, *fliD*, *motB*, *flgM*) in the Δ*tssL2* strain were notably lower than that in the WT and CΔ*tssL2* strains (Fig. 3E). For lateral flagella, the Δ*tssL2* strain showed lower expression of *fliD*, *fliE*, *fliM*, *motB*, and *lafA* than the WT strain (Fig. 3F). These results demonstrated that, under these specific experimental conditions, TssL2 affected the transcription of polar and lateral flagellar genes, resulting in increased swimming and swarming motility.

TssL2 contributes to adhesion and cytotoxicity in vitro

To investigate whether TssL2 affects bacterial pathogenicity, we performed adherence and cytotoxicity tests in Caco-2 cells at MOI of 1:10 (cells: bacteria). For adherence test, Caco-2 cells were infected with the three strains at 1 h. There was significantly 42% reduction in the cell adhesion of the Δ*tssL2* strain, compared to WT strain (Fig. 4A), and the capacities were restored in the complemented strain.

For cytotoxicity test, the lysis of Caco-2 cells infected with strains at an MOI of 1:10 was evaluated in terms of LDH levels. At 2–3 h, the released LDH levels of Caco-2 cells stimulated by the Δ*tssL2* strain were considerably

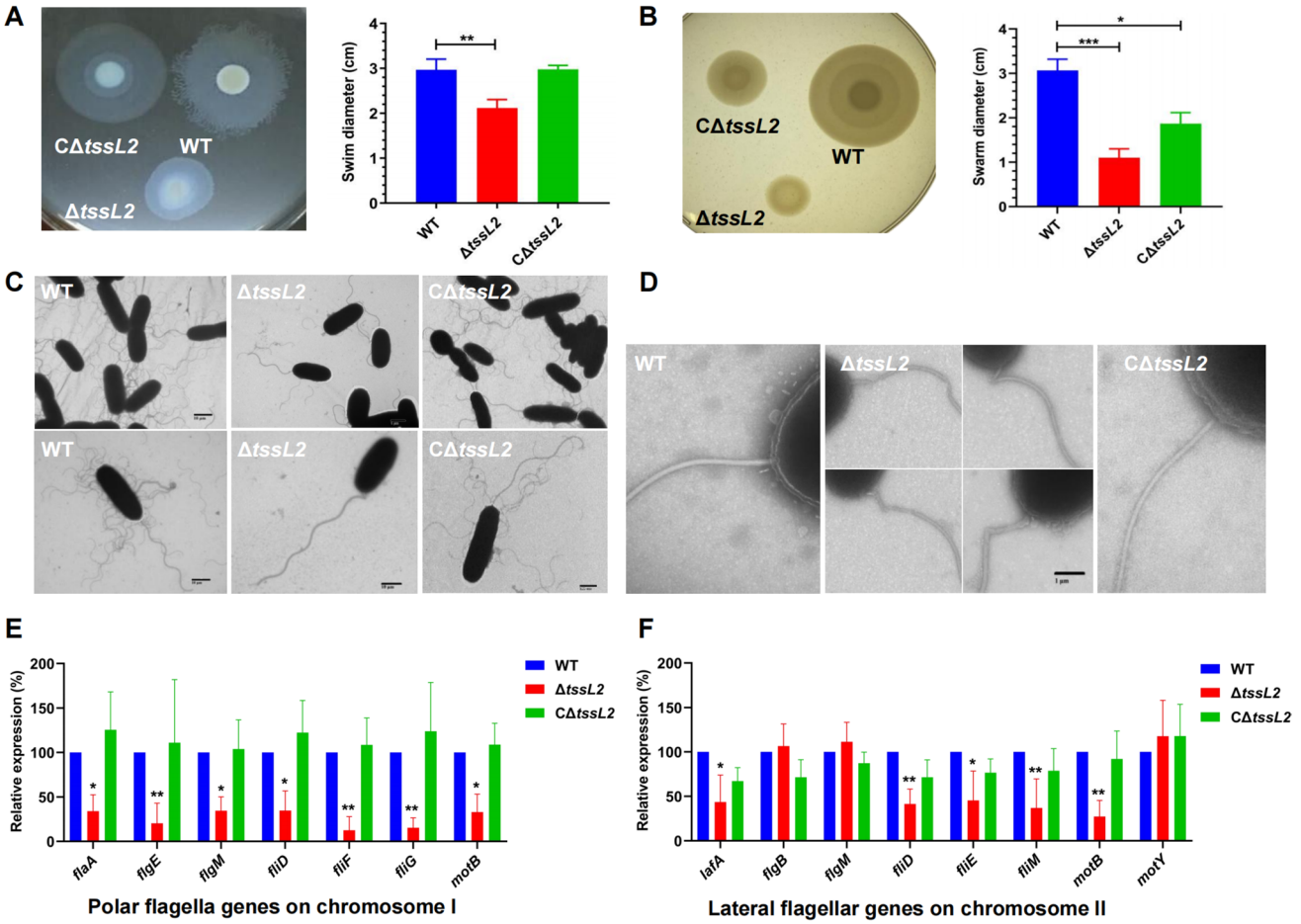

Fig. 3 *TssL2* mutant reduced lateral flagellum- and polar flagellum-mediated motility. **A** Swimming patterns of various *V. parahaemolyticus* strains were analyzed on 0.3% agar-LB plates at 4 h post-incubation, and the swimming diameter (cm) was used to compare differences in the movement of three strains. **B** Swarming patterns were performed on 1.5% agar-HI plates for 24 h. Data analysis was performed using one-way ANOVA, and asterisks indicate that *V. parahaemolyticus* lacking *tssL2* showed significantly weakened swimming and swarming motility, and the CΔ*tssL2* strain restored the swimming motility of the WT strain rather than the swarming motility. **C** Transmission electron microscopy shows the morphology and number of polar and lateral flagella for wild type (WT) and deletion mutant Δ*tssL2* strains (bar = 10 μm). **D** The polar flagellum, especially the basal body (bar = 1 μm), were observed in WT and Δ*tssL2*. The Δ*tssL2* strain had noticeably fewer lateral flagella than the WT strain, with commonly damaged polar flagella. QRT-PCR analysis showed the expression levels of the genes (*flaA*, *flgE*, *flgM*, *fliD*, *fliF*, *fliG*, *motB*) for polar flagella (**E**), and those of the *Laf* genes (*lafA*, *flgB*, *flgM*, *fliD*, *fliE*, *fliM*, *motB*, *motY*) for the lateral flagella (**F**). Data are shown as mean ± SD ($n = 4$) of 2 independent experiments with 2 replicates, using two-way ANOVA, and asterisks denote statistical significance between WT and Δ*tssL2* strains (*$P < 0.05$; **$P < 0.01$; ***$P < 0.001$)

lower than those of the WT and CΔ*tssL2* strains (Fig. 4B). These data suggested that TssL2 contributed to cell adhesion and toxicity of *V. parahaemolyticus* SH112 in vitro.

TssL2 is involved in virulence and colonization in vivo

It has been reported that the *dotU* (*tssL*) mutant has significantly higher LD_{50} values and significantly lower virulence than the WT (Song et al. 2020). To investigate the effect of *V. parahaemolyticus* SH112 TssL2 in virulence in vivo, we compared the LD_{50} values of WT, Δ*tssL2*, and CΔ*tssL2* strains in an ICR mouse model. As indicated by mice mortality over 7 days (Table 1), the LD_{50} values of the WT, Δ*tssL2*, and CΔ*tssL2* strains were 8.42×10^6, 2.38×10^7, and 1.0×10^7 CFU, respectively. These results indicated that the virulence of the Δ*tssL2* strain was greatly reduced compared to that of WT. Moreover, we noticed that the group injected with the WT strain showed more severe clinical symptoms than those injected with the Δ*tssL2* strain from 10 to 20 h post-infection, such as depression, disheveled hair, diarrhea, and/or occasional blood in the urine, indicating acute infection.

To further confirm the role of TssL2, we assessed the survival rate of mice infected by the three strains with an intermediate dose (1.5×10^7 CFU per animal). The survival

rate of mice infected by the Δ*tssL2* strain (75%, 9/12) was markedly higher than that of mice infected by the WT strain (25%, 3/12) (Fig. 4C). Based on the above experiments, we selected time points at 20 h post-infection to detect bacterial colonization in mouse organs. The titers of Δ*tssL2* were lower than that of WT in blood, liver, and spleen samples at 20 h (Fig. 4D) post-infection. The titers of the CΔ*tssL2* strain did not return to the WT level in the liver and spleen. These results showed that TssL2 was critical to colonization and virulence during acute infection in vivo.

TssL2 affects the release of IL-6, IL-8 cytokines upon *V. parahaemolyticus* infection

Caco-2 cells were infected with the three strains at an MOI of 1:100 to analyze the effect of TssL2 on cytokine release. Compared with that observed after WT infection, IL-6 mRNA expression at 3 h and 4 h, and IL-8 mRNA expression at 2 h and 3 h (Fig. 4E) were significantly downregulated in Caco-2 cells after Δ*tssL2* infection. Our results showed that TssL2 regulated IL-6, IL-8 cytokine expression in *V. parahaemolyticus*-infected Caco-2 cells.

TssL2 influences various expression profiles of *V. parahaemolyticus*

To identify secreted proteins of *V. parahaemolyticus* affected by TssL2, we used mass spectrometry to analyze proteomic differences between the Δ*tssL2* and WT strains using label-free quantification (LFQ). As shown in Fig. 5A, 855 secretory proteins in the culture supernatant were identified both in the Δ*TssL2* and WT strains. In addition, 39 proteins were absent in the Δ*tssL2* strain, whereas 30 proteins were absent in the WT strain. Compared with those in WT, 100 secretory proteins were significantly downregulated and 63 were upregulated in Δ*tssL2* ($P < 0.05$) (Table S4). Hierarchical clustering analysis of secretory proteins in the WT and Δ*tssL2* groups is shown in Fig. 5B. The DEPs indicated that many functions were affected through mechanisms involving T6SS2.

To understand the functions of these proteins and to identify the enriched metabolic and signal transduction pathways, we performed gene ontology (GO) term and Kyoto Encyclopedia of Genes and Genomes (KEGG) pathway analysis of the DEPs (Fig. 5C, D). For the GO term enrichment analysis of the DEPs, we focused on molecular function (MF) and biological process (BP) terms. The DEPs of the Δ*tssL2* and WT strains were primarily enriched for BP terms related to DNA-recombination, nitrogen cycle metabolic process, negative regulation of gene expression, and metabolic process. In the case of MF terms, the DEPs were primarily involved in hydrolase activity, nucleoside-triphosphatase activity, transmembrane signaling receptor activity, and ion channel activity.

The DEPs were enriched in KEGG pathways primarily involved in ATP-binding cassette (ABC) transporters and homologous recombination. Eleven proteins involved in ABC transporter system were significantly downregulated in the Δ*tssL2* strain. In addition, 5 proteins involved in flagellar assembly system, and 5 proteins involved in two-component systems were downregulated; conversely, expression levels of 4 proteins involved in biofilm formation and 5 proteins involved in quorum sensing (QS) were upregulated, such as CalR (VP0350) detected only in the Δ*tssL2* but not in WT strain. Furthermore, the major DEPs identified in these two strains were enriched in microbial metabolism pathways, including metabolism of pyrimidine, purine, pyruvate, glycolysis, starch, sucrose, nitrogen, propanoate, and fatty acids. Overall, these results suggested that TssL2 plays an important role in multiple functions and metabolic pathways in *V. parahaemolyticus*.

TssL2 is related to T3SS1 and T2SS transcription

To investigate whether TssL2 affects transcription levels of T3SS1 and T2SS genes, we performed qRT-PCR assays. The results showed that transcription levels of T3SS1 genes (*vopD*, *vopB*, *vscP*, *vecA*, *vopR*, *vopS*, *vscJ*, *vscG*) and T2SS genes (*gspC*, *gspE*, *gspJ*, *gspL*, *gspM*) in Δ*tssL2* strain significantly decreased relative to WT, and transcription levels of in CΔ*tssL2* and WT strains have no significant difference (Fig. 6A, B). The results suggested that TssL2 had positive correlation with the transcription of T3SS1 and T2SS genes.

Discussion

T6SSs are widespread in the genomes of gram-negative bacteria (more than 25%) and are involved in a broad range of functions, including maintenance of bacterial cohabitation, stable ecosystems, environmental stress responses, and virulence (Coulthurst 2019). As a conserved structural protein, TssL (*dotU*) is essential for T6SS assembly and function, and vital for virulence, intracellular life cycle an essential, biofilm formation, invasiveness (Bröms et al. 2012; Song et al. 2020). It was reported that the expression of *dotU* gene in virulent strain was significantly higher than that of attenuated strain and non-virulent strain, suggesting that DotU may be closely related to the virulence regulation (Song et al. 2020). In *V. parahaemolyticus*, TssL1 and TssL2 are components of T6SS1 and T6SS2, respectively. Currently, there are few functional studies on T6SS2, and to the best of our knowledge, there are no studies on the functional consequences of *tssL2* deletion in *V. parahaemolyticus*. Therefore, based on the data of the Δ*tssL2* mutant and complement

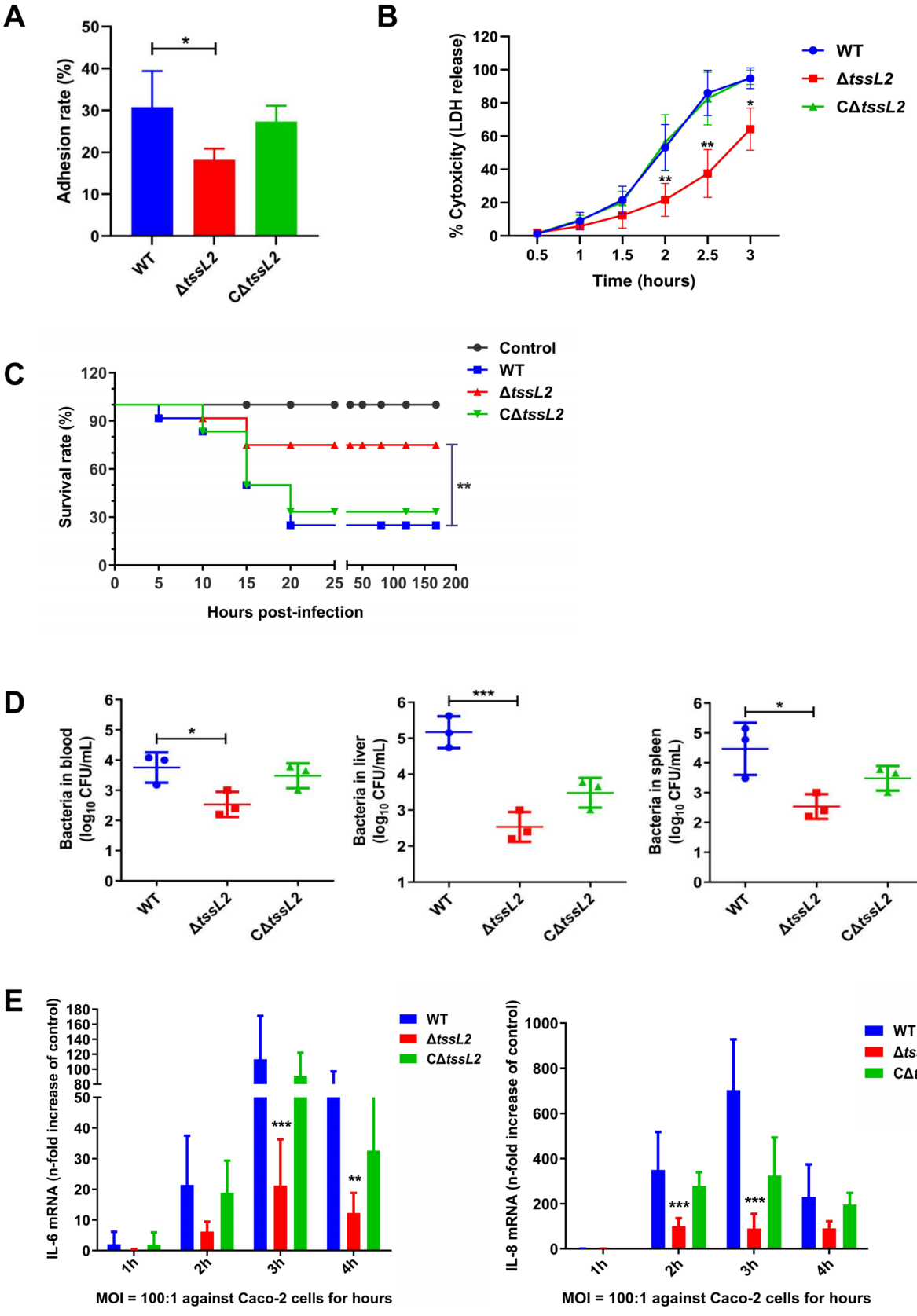
A
Adhesion rate (%)
WT
ΔtssL2
CΔtssL2
B
% Cytoxicity (LDH release)
Time (hours)
WT
ΔtssL2
CΔtssL2
C
Survival rate (%)
Hours post-infection
Control
WT
ΔtssL2
CΔtssL2
D
Bacteria in blood (log10 CFU/mL)
Bacteria in liver (log10 CFU/mL)
Bacteria in spleen (log10 CFU/mL)
E
IL-6 mRNA (n-fold increase of control)
MOI = 100:1 against Caco-2 cells for hours
IL-8 mRNA (n-fold increase of control)
MOI = 100:1 against Caco-2 cells for hours

◂**Fig. 4** *TssL2* gene loss affects adherence, cytotoxicity, colonization of *V. parahaemolyticus*, and cytokine expression in *V. parahaemolyticus*-infected Caco-2 cells. **A** Adhesion of WT, Δ*tssL2*, and CΔ*tssL2* strains to Caco-2 cells. Values represent the mean ± SD ($n=4$) of 2 independent experiments with 2 replicates, and statistical difference was detected with one-way ANOVA (*$P<0.05$). **B** Percent cytotoxicity was assessed by calculating LDH in Caco-2 cells infected by three strains. The data are displayed with the means ± SD ($n=6$) of 2 independent experiments with 3 replicates, and statistical comparisons were performed with two-way ANOVA (*$P<0.05$; **$P<0.01$). **C** The survival rates of four-week-old ICR mice infected intraperitoneally with WT, Δ*tssL2*, and CΔ*tssL2* strains and physiological saline (control group). Asterisks indicate statistical significance between WT and Δ*tssL2* strain by log-rank test. **D** Viable bacterial loads in the blood, liver, and spleen tissues of infected mice ($1.5\times10.^7$ bacteria per animal) at 20 h. Data are means and SD ($n=3$ replicates), and statistically significant differences between WT and Δ*tssL2* strains were detected with one-way ANOVA (*$P<0.05$; **$P<0.01$; ***$P<0.001$). **E** IL-6 and IL-8 expression in bacteria-infected Caco-2 cells analyzed at 1, 2, 3, and 4 h using qRT-PCR. Data were normalized to β-actin expression and calibrated to uninfected Caco-2 cells. Data are means and SD ($n=6$) of 2 independent experiments with 3 replicates, and significant differences between WT and Δ*tssL2* strains were assessed with two-way ANOVA (**$P<0.01$; ***$P<0.001$)

strains of *V. parahaemolyticus* SH112, we analyzed the effects of TssL2 on biofilm formation, colony morphology, motility, flagella formation, bacterial competition, cytotoxicity, colonization, mouse mortality and macrophage cytokine expression, in order to explore the regulatory mechanism of *tssL2* gene on bacterial adaptation and pathogenicity.

As a structural protein and a transporter, Hcp is often used as the hallmark component of functional T6SS (Singh and Kumari 2023; Yu et al. 2012). TssL, as an important component of T6SS, may affect the secretion of Hcp and effectors by affecting the structural integrity of T6SS, rather than affecting the expression of Hcp or other effectors (Lin et al. 2014; Yang et al. 2018). As expected, *tssL2* deletion greatly reduced Hcp2 secretion, and had no effect on transcription of T6SS2 genes, consistent with previous studies in *E. coli* (Wang et al. 2014). These show that TssL2 is essential for T6SS2 activity in *V. parahaemolyticus* SH112. It is worth noting that the cellular Hcp2 secretion was reduced in Δ*tssL2*, while Hcp2 expression at the transcriptional level was though showed a little reduction, but not siganificant in Δ*tssL2*. We suspect there are two main reasons. On the one hand, TssL is embedded in the inner cell membrane and extends across the periplasm to stabilize the plasma membrane (Cherrak et al. 2019). We hypothesized that *tssL2* deletion affected the secretion of Hcp2 as *tssL2* deletion destroyed the structural integrity of T6SS2. On the other hand, DsbA, as a disulfide oxidoreductase, is involved in the stability and assembly of the Dot/Icm complex and subsequently regulates the toxic effects of T6SS effectors on the target cell (Mariano et al. 2018). Proteomic analysis indicated that DsbA protein VPA0546 was detected in the deletion strain but not in the wild strain, suggesting a feedback regulation of TssL2 deletion for enhanced Dot/Icm stability and assembly. Interestingly, inner membrane protein TssL2 of T6SS2 had significant effects on 36 membrane-related proteins, including 11 ABC transporter proteins and 25 membrane-bound proteins. ABC systems play various biological roles in substrate transport, efflux, acquisition, uptake, and membrane integrity or stability (Chen and Duan 2016). In *Pseudomonas aeruginosa*, ABC-transporters are important in surface-induced phosphorylation and T6SS activation (Casabona et al. 2013). The above results can help to indicate that TssL2 may affect other membrane integrity or stability structures, including T6SS2 stability, causing a small amount of Hcp2 to be secreted outside the cell, thereby reducing the level of Hcp2 protein in the cell.

In *V. fluvialis* (Huang et al. 2017; Pan et al. 2018), T6SS2 associates with antibacterial activity via the Hcp2-dependent pathway. Recently, several T6SS2-secreted effectors and Hcp2 have been shown to be involved in interbacterial competition of *V. parahaemolyticus* (Tchelet et al. 2023). Similar to *hcp2* (see Fig. S3 in the supplemental material), *tssL2* deletion of *V. parahaemolyticus* SH112 significantly affected bacterial VpT6SS2-mediated killing in vitro, which is consistent with the results obtained for *V. alginolyticus* (Yang et al. 2018), strongly confirming that TssL2 is essential for Hcp2 secretion, thereby contributing to interbacterial competition.

Vibrio spp. have strong biofilm-forming ability, which could involve in environmental survival and bacterial pathogenesis (Mizan et al. 2016; Silva and Benitez 2016). Biofilm production of Δ*tssL2* strain was 3.2-fold higher than that of WT; similar results have been reported in *Aeromonas veronii* where Δ*dotU* exhibited 2.1-fold greater biofilm formation than WT (Song et al. 2020). Besides, the *hcp2* mutant increased biofilm production in *V. parahaemolyticus* (see Fig. S4 in the supplemental material), consistent with previous studies (Wang et al. 2018a, b). These results suggested that T6SS2 may be involved in biofilm formation. Biofilm formation is a complex and dynamic process in which assembled communities of microorganisms are surrounded by extracellular polysaccharides (EPS) (Giacomucci et al. 2019). Expression and production of EPS contribute to biofilm formation, which is regulated by QS and cyclic di-GMP (c-di-GMP) (Jung et al. 2019). AphA and OpaR, as QS regulators, activate and inhibit biofilm formation under low cell density and high cell density conditions, respectively (Sun et al. 2022). Our data showed that *tssL2* deletion positively and negatively regulated *aphA* and *opaR* transcription, respectively. However, the regulatory mechanisms need to be further studied. Moreover, in Δ*tssL2* strain, c-di-GMP-related genes (*cpsQ*, *mfpA*) were significantly positively regulated. CpsQ, as a c-di-GMP-binding protein, positively regulates expression of capsular polysaccharide

Table 1 LD_{50} of *V. parahaemolyticus* SH112 wildtype, *tssL2* deletion, and complementation strain for ICR mice

Number of deaths/total				Mortality (%)		
Dose of challenge CFU	WT	Δ*tssL2*	CΔ*tssL2*	WT	Δ*tssL2*	CΔ*tssL2*
4×10^7	8/8	1/8	8/8	100%	87.5%	100%
2×10^7	8/8	3/8	6/8	100%	37.5%	75.0%
1×10^7	5/8	1/8	4/8	62.5%	12.5%	50.0%
5×10^6	1/8	0/8	2/8	12.5%	0%	25.0%
2.5×10^6	0/8	0/8	0/8	0%	0%	0%
LD_{50}				8.42×10^6	2.38×10^7	1.0×10^7

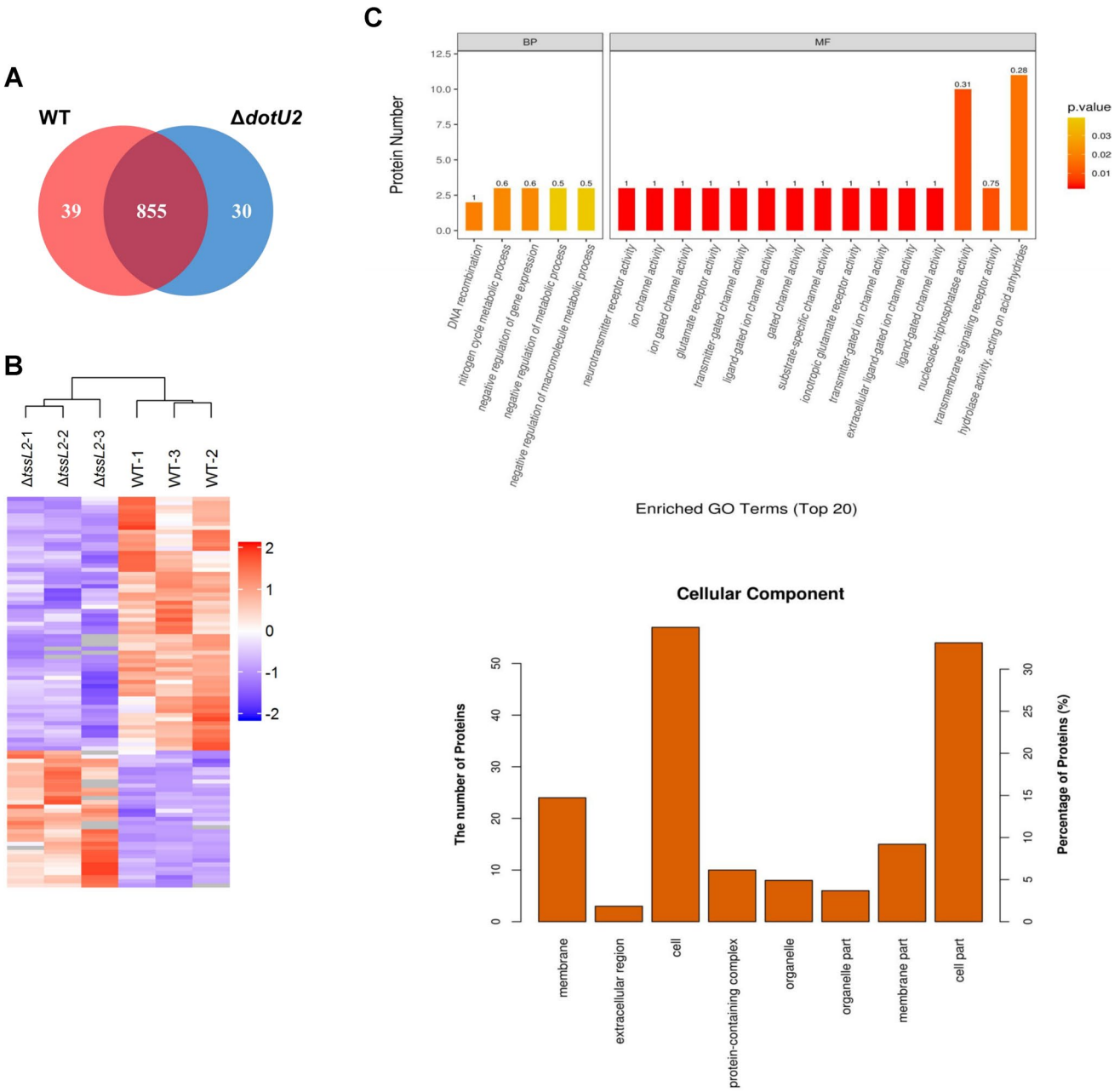

Fig. 5 Bioinformatics analysis of TssL2-dependent secretion in *V. parahaemolyticus* identified by label-free mass spectrometry. **A** The number of identified proteins from WT and Δ*tssL2* group. **B** Hierarchical clustering, **C** GO terms, and **D** KEGG pathway analysis of DEPs in two groups. Bar color represents a logarithmic scale from − 2 to 2

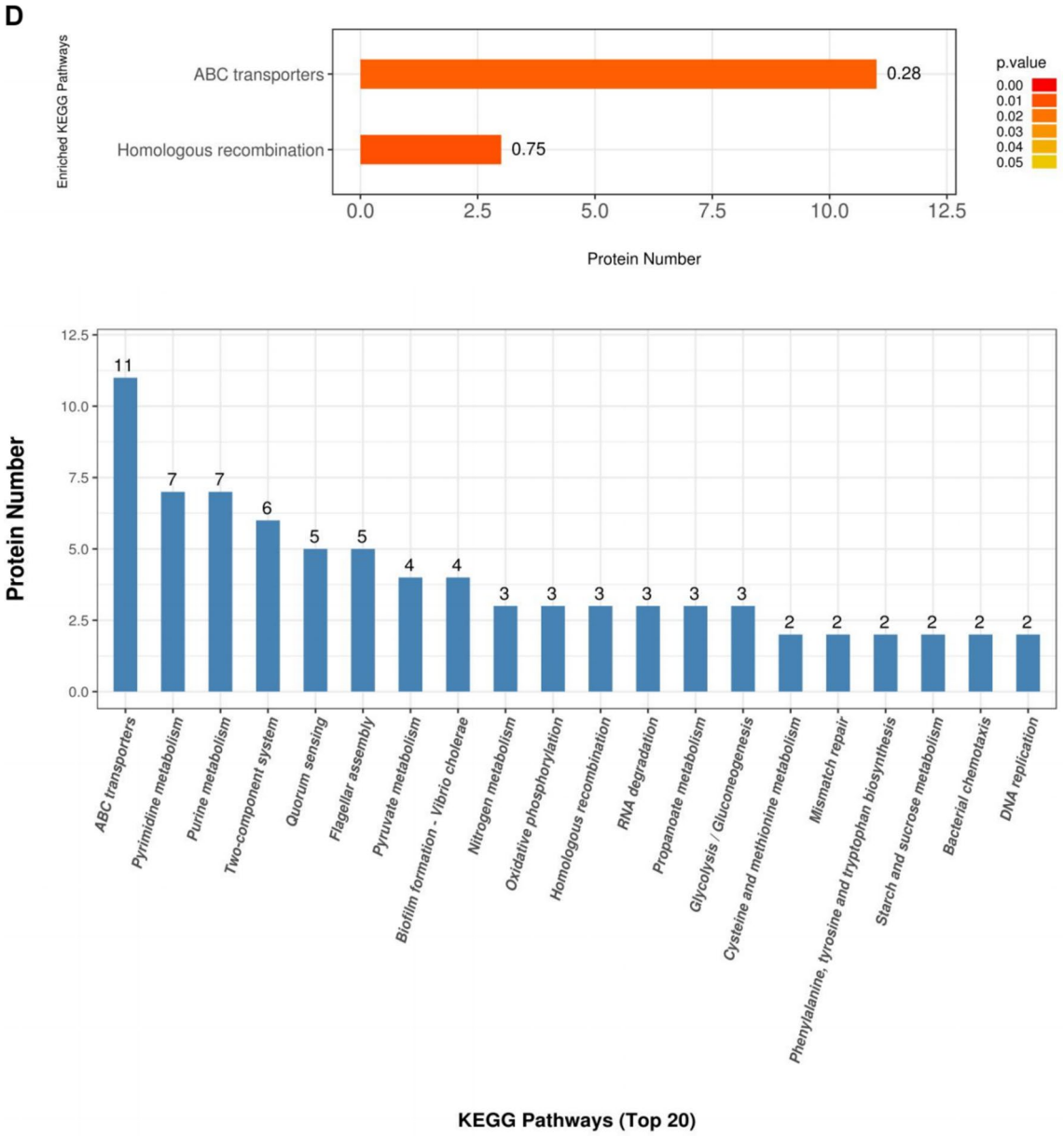

Fig. 5 (continued)

(CPS, a component of EPS) genes and *mfpABC*, contributes to biofilm development of *V. parahaemolyticus* (Zhou et al. 2013a, b). CalR, as a LysR-type transcriptional regulator, directly activates *cpsQ* and *mfpABC* transcription in *V. parahaemolyticus* (Gao et al. 2017). TssL2 loss significantly enhanced transcription and expression of *calR* (VP0350) gene, suggesting that TssL2 deletion may positively regulate transcription levels of *cpsQ* and *mfpABC* by CalR pathway, leading to the promotion of EPS production and biofilm formation. It was worth noting that the generation of EPS and biofilm were known mechanisms of resistance to T6SS's contact-dependent attacks during bacterial competition (Flaugnatti et al. 2021; Dessartine et al. 2024). The resistance mechanism may be due to the EPS forming a physical barrier or due to the biofilm forming a barrier of dead cells and debris at the attactor-target interface (Dessartine et al. 2024). Whether TssL2 contributes to interbacterial competition is related to the reduction of EPS and biofilm production is worth further study.

Motility is essential for bacterial survival in various environments and increases virulence upon reaching the target host site, adhesion to cells or surfaces, colonization, maintenance of infection, and dispersal (Zegadlo et al. 2023; Qiao et al. 2022). Bacterial motility occurs via flagella. *Vibrio* spp. depend on dual flagellar systems to adapt to different environments; the single polar flagellum enables swimming

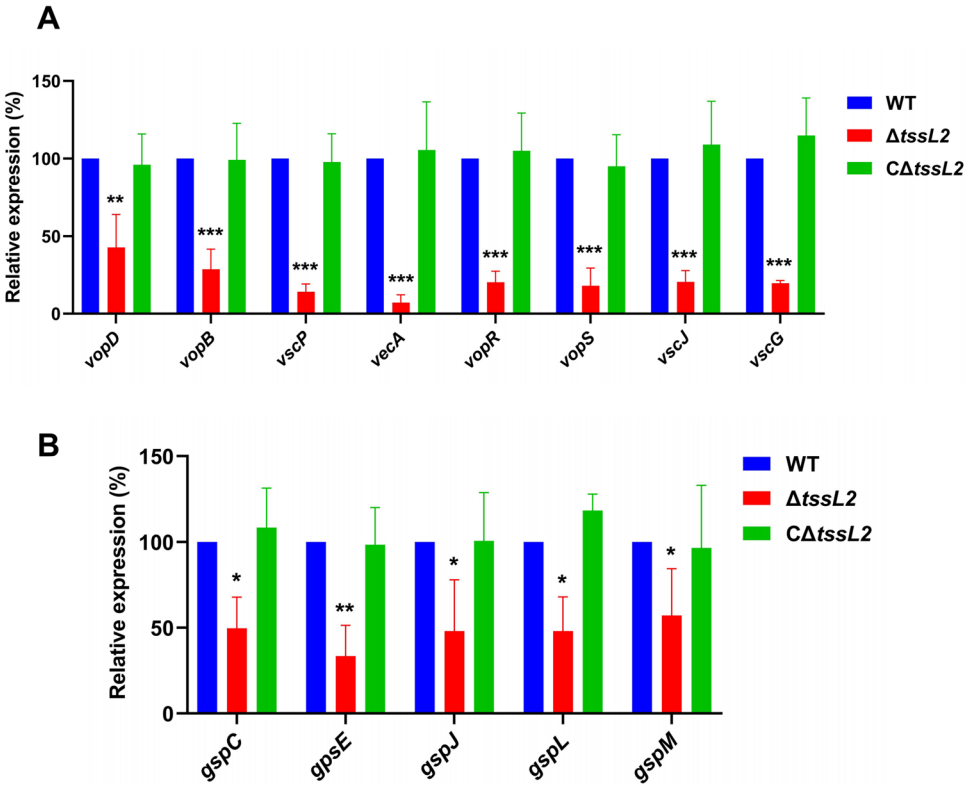

Fig. 6 Mutation in *tssL2* represses transcription of T3SS1 and T2SS genes. **A** The relative mRNA levels of T3SS1 genes (*vopD*, *vopB*, *vscP*, *vecA*, *vopR*, *vopS*, *vscJ*, *vscG*) were compared between WT, Δ*tssL2*, CΔ*tssL2* strains. **B** The relative mRNA levels of T2SS genes (*gspC*, *gspE*, *gspJ*, *gspL*, *gspM*) were compared between three strains. Data are shown as mean ± SD ($n = 4$) from 2 independent experiments with 2 replicates, using two-way ANOVA, and asterisks denote statistical significance between WT and Δ*tssL2* strains (*$P < 0.05$; **$P < 0.01$; ***$P < 0.001$)

in a liquid environment, and the lateral flagella enables swarming and colonization on viscous surfaces (McCarter 2004). *TssL2* deletion leads to the weakened motility of *V. parahaemolyticus* SH112, whether for swimming or swarming. Moreover, similar results occurred in *hcp2* (see Fig. S5 in the supplemental material). These results suggested that *tssL2* deletion inhibited bacterial motility due to T6SS2 deficiency, which is consistent with the findings in *V. cholerae* (Frederick et al. 2020), APEC (de Pace et al. 2011), and *Acidovorax avenae* (Masum et al. 2017). To further explore the impact of TssL2 on flagellar-mediated motility, TEM was used to observe the bacterial flagella of the three strains. As expected, micrographs of Δ*tssL2* had more severely damaged polar flagella and fewer lateral flagella than those of WT. The regulation for polar and lateral flagella formation and function are complex. The polar flagellar genes were grouped into three hierarchies: early, middle, and late (Noh et al. 2015). The qRT-PCR results showed that the damage to the polar flagellum was due to the weakened expression of the middle (*flgE*, *fliF*, and *fliG*) and late genes (*flaA*, *fliD*, *motB*, and *flgM*), and the lateral flagellum defect was due to the regulatory regions of the *Laf* genes (Lu et al. 2019) being affected. However, why were lateral flagellum genes *flgB*, *flgM*, and *motY* not affected by TssL2, deserving further investigation. Consistent with these results, proteomic data showed that loss of TssL2 leads to the pronounced downregulation of 5 polar flagellar proteins (FlaA, FlgM, FlgK, FlgB, and FliL) in a fluid medium. These results verified that TssL2 affects bacterial motility by regulating polar and lateral flagellar expression and assembly. As the flagella systems of *V. parahaemolyticus* are extremely complex, how TssL2 of T6SS2 affects or regulates flagellar genes remains to be solved.

Cell–cell crosslinking and aggregation may enable bacteria to exist as tight communities, thereby aiding the survival and colonization of bacteria in the host and contributing to protective immunity during infection (Baranova et al. 2018). Bacterial aggregation, or formation of non-surface-associated communities in liquid, is typically associated with QS, pilus, motility, polysaccharides, adhesins, colonization, and the bacterial passage rate through the intestine (Jemielita et al. 2018; Levinson et al. 2015). Our results suggested that the *tssL2* deletion contributed to cell aggregation in a static liquid medium. Xiu et al. (2018) and Dalili et al (2015) previously used cell aggregation in liquid culture to evaluate wrinkled colony and biofilm formation in *Vibrio* (Xiu et al. 2018) and *Corynebacterium xerosis* (Dalili et al. 2015). In addition, increased bacterial aggregation in vitro can be affected by flagellum-flagellum cross-linking, pilus, polysaccharide, and adhesins, but it is also a potent inhibitor of bacterial motility (Levinson et al. 2015). Whether the elevated biofilm formation and defective motility caused by TssL2 loss are related to cell aggregation requires further exploration.

V. parahaemolyticus reversibly switches between wrinkly and smooth phenotypes to adapt to changing environments

(Wu et al. 2022). During this process, gene expressions of multiple pathways were significantly regulated, related to T6SS2, T3SS1, flagellar synthesis, biofilm formation, metabolism, and colonization (Wu et al. 2022). In contrast to WT, which had smooth and opaque colonies (smooth phenotype), *tssL2* mutant colonies were rugose and translucent (wrinkly phenotype). Besides, *hcp2* mutant exhibited a similar wrinkly phenotype (see Figure S6 in the supplemental material), suggesting that *tssL2* deletion was beneficial to smooth-wrinkly phenotype switching, which may be related to T6SS2 inactivation. In addition, our data showed that *tssL2* deletion downregulated expression of T3SS1 genes (*vopD*, *vopB*, *vscP*, *vecA*, *vopR*), putative regulators (RpoS), polar flagellar gene (*flgM*), lateral flagellar genes (*lafA*, *fliD*, *fliE*, *fliM*, *motB*), and upregulated expression of biofilm-related genes (*cpsQ*, *aphA*), metabolism-related proteins (VP1647, VP1626, VPA0472), uncharacterized proteins (VP1279, VPA0668, VP1444, VPA1308), and which were consistent with the previous results (Wu et al. 2022). Therefore, another mechanism is that TssL2 deficiency changes smooth phenotype to wrinkly phenotype by influencing T3SS1, flagella synthesis, biofilm and other ways (Fig. 7).

The T6SS2 has been shown to contribute to adhesion and cytotoxicity to host cells (Liu et al. 2015; Soria-Bustos et al. 2020). TssL was reported to be involved in cell adhesion ability (Le Goff et al. 2022). We found that TssL2 loss significantly decreased bacterial adhesion and cytotoxicity. Similarly, *hcp2* mutant hampered cell adhesion and cytotoxicity (see Fig. S7 in the supplemental material), consistent with the study results that Hcp2 reduced adhesion and toxicity (Wu et al. 2023). These results suggest that TssL2 contributes to cell adhesion and cytotoxicity by T6SS2 activation. However, this result is inconsistent with a published study by Yu et al. (2012; 2015), wherein the T6SS2 of *V. parahaemolyticus* contributed to cell adhesion without causing cytotoxicity. The difference in the deletion strains, where we used *tssL2*

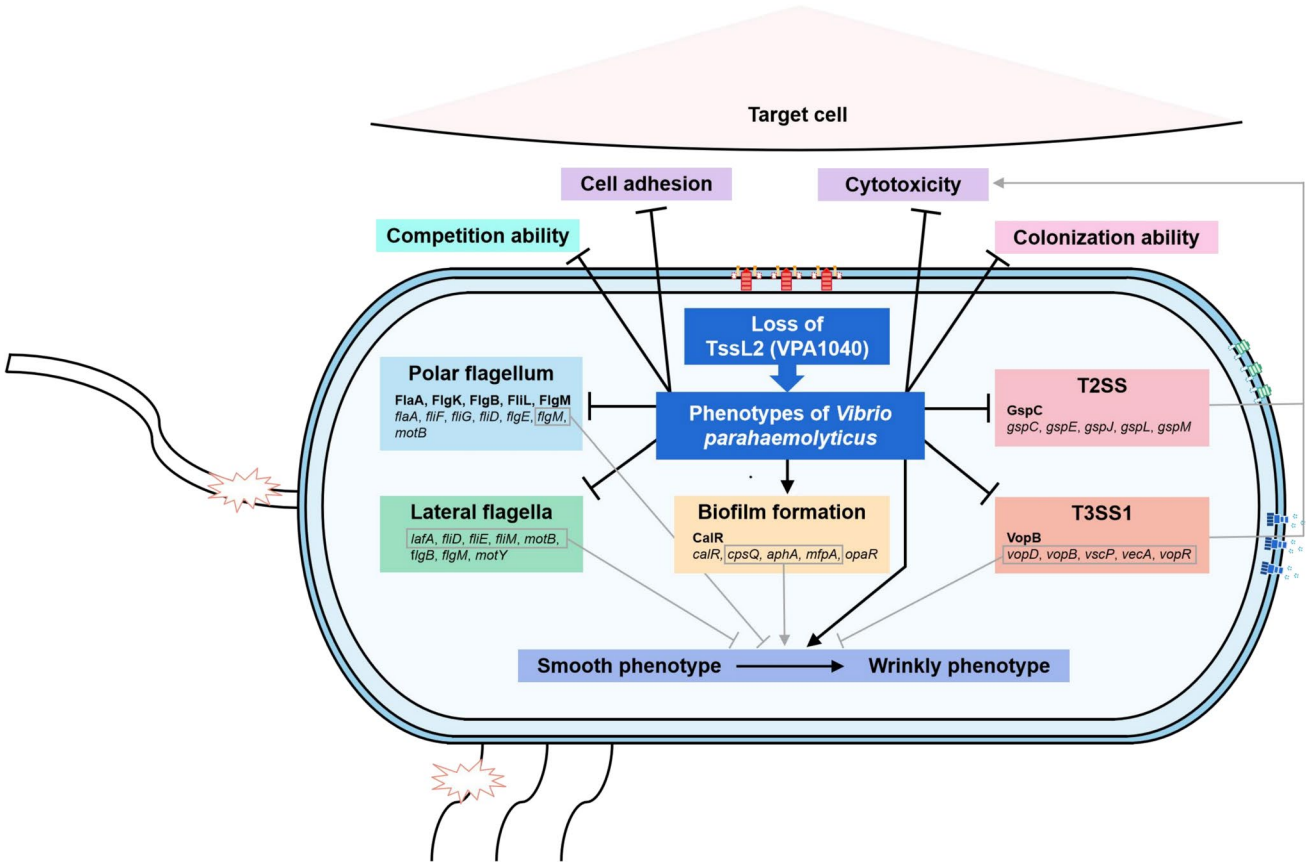

Fig. 7 Regulatory network of TssL2 inactivation in effect of environmental adaption and virulence. Loss of TssL2 in T6SS2 changed the phenotype of *Vibrio parahaemolyticus*, leading to inhibition of competition ability, flagellar synthesis, T3SS1, T2SS, cell adhesion, cytotoxicity, colonization, promotion of biofilm, and wrinkly phenotype formation. Arrows indicate positive regulation, and vertical lines indicate negative regulation. Moreover, downregulated polar flagellar gene (*flgM*), lateral flagellar genes (*lafA*, *fliD*, *fliE*, *fliM*, *motB*), T3SS1 genes (*vopD*, *vopB*, *vscP*, *vecA*, *vopR*), and upregulated expression of biofilm-related genes (*cpsQ*, *aphA*, *mfpA*) have positive effects on wrinkly phenotype formation, as described in previous studies. The sections described in the previous study are represented in gray lines, and those described in the current study are represented in black lines

mutant and Yu et al. (2015) used *tssL2* mutant, might explain this disparity in results. In addition, we found *tssL2* deletion significantly reduced transcription levels of T3SS1 and T2SS genes, consistent with *hcp2* mutant (see Fig. S8 in the supplemental material). And *tssL2* deletion was confirmed by reduced expression of VopB in T3SS1 and GspC in T2SS using proteomic analysis. T3SS1 is responsible for cytotoxicity in *V. parahaemolyticus* infection (Shimohata et al. 2012), and T2SS aids in the secretion of exoproteins including virulence factors (Reichow et al. 2011). Another possibility is that TssL2 affects other virulence-related factors, including T3SS1 and T2SS, thus alters bacterial virulence.

Currently, T6SS2 was proved to be involved in cell colonization (Soria-Bustos et al. 2020; Schmidt et al. 2023; Wang et al. 2022). To further reveal the functions of TssL2, bacterial colonization and murine mortality were investigated, as these are important virulence parameters for infection and pathogenesis (Wang et al. 2014; Gao et al. 2013). Our results revealed that *tssL2* deletion caused weakened virulence and lower mortality in mice, similar to previous studies of *E. coli* (Wang et al. 2014). This may be a strong signal that TssL2 plays an important role in bacterial virulence by activating T6SS2. In addition, TssL was reported to affect cytokine production in *E. coli* (Wang et al. 2014). As important inflammatory mediators, IL-6 and IL-8 expression levels are affected by TssL2 during infection. Proteomic analysis showed that TssL2 affects the cytokine production levels via other proteins, such as the downregulation of VopB and upregulation of OmpA, which were reported to be essential for IL-8 secretion (Shimohata et al. 2012; March et al. 2011). We speculate that TssL2 might enable *V. parahaemolyticus* SH112 to enhance cytotoxicity, leading to the production of cytokines that regulate inflammation while also damaging host immune cells to allow evasion, colonization, and tissue infection, leading to increased survival.

Here, our results showed that TssL2 of T6SS2 not only significantly affects bacterial adaptation, including competition ability, swimming and swarming motility, biofilm formation, and colony morphology, but also regulates with T3SS1 and T2SS, and contributes bacterial pathogenicity in vitro and in vivo, including bacterial cytotoxicity, colonization, virulence. Especially, proteome analysis supports the effect of TssL2 on the different phenotypes of *V. parahaemolyticus*. The results of wrinkly phenotype formation caused by TssL2 deficiency validate that TssL2 is associated with multiple pathways, including T3SS1, flagellar synthesis, biofilm (Fig. 7). In addition, based on the results, we propose a regulatory circuit for TssL2 loss involving regulation of swarming motility, biofilm formation, virulence by CalR pathway. CalR was reported to repress transcription of T3SS1 and lateral flagellar genes in *V. parahaemolyticus* (Osei-Adjei et al. 2017; Gu et al. 2019), suggesting that the elevated CalR caused by TssL2 deficiency may be responsible for decreased expression of T3SS1 and lateral flagellar genes, thereby controlling T3SS1-dependent cytotoxicity and swarming motility. Meanwhile, elevated CalR may also be responsible for the elevated biofilm by regulating *cpsQ-mfpABC* transcription (Zhou et al. 2013a, b). In addition, CalR was shown to be a positive regulator of T6SS2 expression in *V. parahaemolyticus* (Zhang et al. 2017a, b). Our results show that the TssL2 loss leads to increased CalR transcription and expression, reflecting a potential feedback regulatory mechanism. In addition, our findings also confirmed that most of the roles of Hcp2 and TssL2 in affecting the function of *V. parahaemolyticus* were consistent. These data give us a hint that these phenotypes maybe contributed by the lack of T6SS2 function due to decreased Hcp2 secretion. Moreover, TssM (IcmF) is also a key molecule of membrane complex for T6SS assembly and have been reported to be largely associated with various biological functions such as bacterial virulence, biofilm formation and resistance to different environments (Wang et al. 2019; Li et al. 2018). And DotU (TssL) has been found to interact with IcmF in several bacteria (Lin et al. 2014). Therefore, whether the interaction of TssL2 and TssM2 result in the changes of membrane structure and the influence of a series of functions is worth further studying, which will be the focus of our future research. Overall, these results expand our knowledge on the roles of T6SS2 components in bacterial virulence and environmental adaptation, and form the basis for further research on *V. parahaemolyticus* infection and effect on the host's immune response.

Supplementary Information The online version contains supplementary material available at https://doi.org/10.1007/s00253-024-13351-8.

Author contribution XRB: methodology, project administration, visualization, writing—original draft, writing—review and editing; WJ: conceptualization, methodology, formal analysis, project administration, funding acquisition, writing—design and review; XGH: writing—review and editing; PXL: methodology, investigation; WCW, YHJ, YQ: methodology; QW: methodology, supervision; XYZ: methodology, visualization; WDS: visualization; WHF: methodology.

Funding This study was funded by the National Natural Science Foundation of China (grant no. 32473039; 31702277), the Shanghai Natural Science Foundation of China (grant no. 21ZR1477000; 17ZR1447200), the Shanghai Science and Technology Commission Research Project (grant no. 21N31901000), the Basic Foundation for Scientific Research of State-level Public Welfare Institutes of China (no. 2020JB07), the Shanghai Chenguang Project (grant no. KY3-0102-18-01) and College-level Project (grant no. KY2-0000-20-10).

Data availability All data included in this study are available upon request by contacting the corresponding author.

Declarations

Ethics approval All applicable international, national, and institutional animal care and use guidelines were followed. The animal experiments were approved by the Animal Ethics Committee of the Shanghai Veterinary Research Institute, Chinese Academy of Agricultural Sciences (no. SYXK < HU > 2020–0027).

Conflict of interest The authors declare no conflict of interest.

References

Ashrafudoulla M, Mizan MFR, Park H, Byun KH, Lee N, Park SH, Ha SD (2019) Genetic relationship, virulence factors, drug resistance profile and biofilm formation ability of *Vibrio parahaemolyticus* isolated from mussel. Front Microbiol 10:513. https://doi.org/10.3389/fmicb.2019.00513

Baranova DE, Levinson KJ, Mantis NJ (2018) *Vibrio cholerae* O1 secretes an extracellular matrix in response to antibody-mediated agglutination. PLoS ONE 13:e0190026. https://doi.org/10.1371/journal.pone.0190026

Bröms JE, Meyer L, Lavander M, Larsson P, Sjöstedt A (2012) DotU and VgrG, core components of type VI secretion systems, are essential for *Francisella* LVS pathogenicity. PLoS ONE 7:e34639. https://doi.org/10.1371/journal.pone.0034639

Casabona MG, Silverman JM, Sall KM, Boyer F, Coute Y, Poirel J, Grunwald D, Mougous JD, Elsen S, Attree I (2013) An ABC transporter and an outer membrane lipoprotein participate in posttranslational activation of type VI secretion in *Pseudomonas aeruginosa*. Environ Microbiol 15:471–486. https://doi.org/10.1111/j.1462-2920.2012.02816.x

Chen L, Duan K (2016) A PhoPQ-regulated ABC transporter system exports tetracycline in *Pseudomonas aeruginosa*. Antimicrob Agents Chemother 60:3016–3024. https://doi.org/10.1128/aac.02986-15

Cherrak Y, Flaugnatti N, Durand E, Journet L, Cascales E (2019) Structure and activity of the type VI secretion system. Microbiol Spectr 7:7–4. https://doi.org/10.1128/microbiolspec.psib-0031-2019

Coulthurst S (2019) The type VI secretion system: a versatile bacterial weapon. Microbiology (Reading) 165:503–515. https://doi.org/10.1099/mic.0.000789

Dalili D, Amini M, Faramarzi MA, Fazeli MR, Khoshayand MR, Samadi N (2015) Isolation and structural characterization of Coryxin, a novel cyclic lipopeptide from *Corynebacterium xerosis* NS5 having emulsifying and anti-biofilm activity. Colloids Surf B Biointerfaces 135:425–442. https://doi.org/10.1016/j.colsurfb.2015.07.005

De Pace F, Boldrin de Paiva J, Nakazato G, Lancellotti M, Sircili MP, Stehling EG, da Silveira WD, Sperandio V (2011) Characterization of IcmF of the type VI secretion system in an avian pathogenic *Escherichia coli* (APEC) strain. Microbiology (Reading) 157:2954–2962. https://doi.org/10.1099/mic.0.050005-0

Dessartine MM, Kosta A, Doan T, Cascales É, Côté J-P (2024) Type 1 fimbriae-mediated collective protection against type 6 secretion system attacks. mBio 15:e02553-23. https://doi.org/10.1128/mbio.02553-23

Faleye OS, Sathiyamoorthi E, Lee JH, Lee J (2021) Inhibitory effects of cinnamaldehyde derivatives on biofilm formation and virulence factors in *Vibrio* species. Pharmaceutics 13:2176. https://doi.org/10.3390/pharmaceutics13122176

Flaugnatti N, Isaac S, Lemos Rocha LF, Stutzmann S, Rendueles O, Stoudmann C, Vesel N, Garcia-Garcera M, Buffet A, Sana TG, Rocha EPC, Blokesch M (2021) Human commensal gut *Proteobacteria withstand* type VI secretion attacks through immunity protein-independent mechanisms. Nat Commun 12:5751. https://doi.org/10.1038/s41467-021-26041-0

Flood MT, Kondo M (2004) Toxicity evaluation of a beta-galactosidase preparation produced by *Penicillium multicolor*. Regul Toxicol Pharmacol 40:281–292. https://doi.org/10.1016/j.yrtph.2004.07.011

Frederick A, Huang Y, Pu M, Rowe-Magnus DA (2020) *Vibrio cholerae* type VI activity alters motility behavior in mucin. J Bacteriol 202:e00261-e320. https://doi.org/10.1128/JB.00261-20

Gao Q, Xu H, Wang X, Zhang D, Ye Z, Gao S, Liu X (2013) RfaH promotes the ability of the avian pathogenic *Escherichia coli* O2 strain E058 to cause avian colibacillosis. J Bacteriol 195:2474–2480. https://doi.org/10.1128/JB.02074-12

Gao H, Zhang L, Osei-Adjei G, Yang W, Zhou D, Huang X, Yang H, Yin Z, Zhang Y (2017) Transcriptional regulation of cpsQ-mfpABC and mfpABC by CalR in *Vibrio parahaemolyticus*. Microbiologyopen 6:e00470. https://doi.org/10.1002/mbo3.470

Giacomucci S, Cros CD, Perron X, Mathieu-Denoncourt A, Duperthuy M (2019) Flagella-dependent inhibition of biofilm formation by sub-inhibitory concentration of polymyxin B in *Vibrio cholerae*. PLoS ONE 14:e0221431. https://doi.org/10.1371/journal.pone.0221431

Gu D, Meng H, Li Y, Ge H, Jiao X (2019) A GntR family transcription factor (VPA1701) for swarming motility and colonization of *Vibrio parahaemolyticus*. Pathogens 8:235. https://doi.org/10.3390/pathogens8040235

Guo D, Yang Z, Zheng X, Kang S, Yang Z, Xu Y, Shi C, Tian H, Xia X (2019) Thymoquinone inhibits biofilm formation and attachment-invasion in host cells of *Vibrio parahaemolyticus*. Foodborne Pathog Dis 16:671–678. https://doi.org/10.1089/fpd.2018.2591

Han D, Yu F, Chen X, Zhang R, Li J (2019) Challenges in *Vibrio parahaemolyticus* infections caused by the pandemic clone. Future Microbiol 14:447–450. https://doi.org/10.2217/fmb-2018-0308

Huang Y, Du P, Zhao M, Liu W, Du Y, Diao B, Li J, Kan B, Liang W (2017) Functional characterization and conditional regulation of the type VI secretion system in *Vibrio fluvialis*. Front Microbiol 8:528. https://doi.org/10.3389/fmicb.2017.00528

Jemielita M, Wingreen NS, Bassler BL (2018) Quorum sensing controls *Vibrio cholerae* multicellular aggregate formation. Elife 7:e42057. https://doi.org/10.7554/eLife.42057

Jung YC, Lee MA, Lee KH (2019) Role of flagellin-homologous proteins in biofilm formation by pathogenic *Vibrio* Species. mBio 10:e01793-19. https://doi.org/10.1128/mBio.01793-19

Kimbrough JH, Cribbs JT, McCarter LL (2020) Homologous c-di-GMP-binding Scr transcription factors orchestrate biofilm development in *Vibrio parahaemolyticus*. J Bacteriol 202:e00723-e819. https://doi.org/10.1128/JB.00723-19

Le Goff M, Vastel M, Lebrun R, Mansuelle P, Diarra A, Grandjean T, Triponney P, Imbert G, Gosset P, Dessein R, Garnier F, Durand E (2022) Characterization of the *Achromobacter xylosoxidans* type VI secretion system and its implication in cystic fibrosis. Front Cell Infect Microbiol 12:859181. https://doi.org/10.3389/fcimb.2022.859181

Levinson KJ, De Jesus M, Mantis NJ (2015) Rapid effects of a protective O-polysaccharide-specific monoclonal IgA on *Vibrio cholerae* agglutination, motility, and surface morphology. Infect Immun 83:1674–1683. https://doi.org/10.1128/IAI.02856-14

Li B, Wang X, Chen J, Liu H, Ali KA, Wang Y, Qiu W, Sun G (2018) IcmF and DotU are required for the virulence of *Acidovorax oryzae* strain RS-1. Arch Microbiol 200(6):897–910. https://doi.org/10.1007/s00203-018-1497-z

Li Y, Sun W, Wang Q, Yu Y, Wan Y, Zhou K, Guo R, Han X, Chen Z, Fang W, Jiang W (2022) The GntR-like transcriptional regulator HutC involved in motility, biofilm-forming ability, and virulence in *Vibrio parahaemolyticus*. Microb Pathog 167:105546. https://doi.org/10.1016/j.micpath.2022.105546

Lian L, Li W, Xue T, Ren J, Tang F, Liu Y, Xue F, Dai J (2022) Comparative transcriptomic analysis provides insights into transcription mechanisms of *Vibrio parahaemolyticus* T3SS during interaction with HeLa cells. Braz J Microbiol 53:289–301. https://doi.org/10.1007/s42770-021-00627-8

Lin JS, Wu HH, Hsu PH, Ma LS, Pang YY, Tsai MD, Lai EM (2014) Fha interaction with phosphothreonine of TssL activates type VI secretion in *Agrobacterium tumefaciens*. PLoS Pathog 10:e1003991. https://doi.org/10.1371/journal.ppat.1003991

Liu H, Gu D, Sheng L, Wang Q, Zhang Y (2012) Investigation of the roles of T6SS genes in motility, biofilm formation, and extracellular protease Asp production in *Vibrio alginolyticus* with modified Gateway-compatible plasmids. Lett Appl Microbiol 55:73–81. https://doi.org/10.1111/j.1472-765X.2012.03263.x

Liu L, Hao S, Lan R, Wang G, Xiao D, Sun H, Xu J (2015) The type VI secretion system modulates flagellar gene expression and secretion in *Citrobacter freundii* and contributes to adhesion and cytotoxicity to host cells. Infect Immun 83:2596–2604. https://doi.org/10.1128/IAI.03071-14

Lu R, Tang H, Qiu Y, Yang W, Yang H, Zhou D, Huang X, Hu L, Zhang Y (2019) Quorum sensing regulates the transcription of lateral flagellar genes in *Vibrio parahaemolyticus*. Future Microbiol 14:1044–1053. https://doi.org/10.2217/fmb-2019-0048

Ma L, Zhang Y, Yan X, Guo L, Wang L, Qiu J, Yang R, Zhou D (2012) Expression of the type VI secretion system 1component Hcp1 is indirectly repressed by OpaR in *Vibrio* parahaemolyticus. Sci World J 2012:982140. https://doi.org/10.1100/2012/982140

Mala W, Alam M, Angkititrakul S, Wongwajana S, Lulitanond V, Huttayananont S, Kaewkes W, Faksri K, Chomvarin C (2016) Serogroup, virulence, and molecular traits of *Vibrio parahaemolyticus* isolated from clinical and cockle sources in northeastern Thailand. Infect Genet Evol 39:212–218. https://doi.org/10.1016/j.meegid.2016.01.006

March C, Moranta D, Regueiro V, Llobet E, Tomas A, Garmendia J, Bengoechea JA (2011) *Klebsiella pneumoniae* outer membrane protein A is required to prevent the activation of airway epithelial cells. J Biol Chem 286:9956–9967. https://doi.org/10.1074/jbc.M110.181008

Mariano G, Monlezun L, Coulthurst SJ (2018) Dual role for DsbA in attacking and targeted bacterial cells during type VI secretion system-mediated competition. Cell Rep 22:774–785. https://doi.org/10.1016/j.celrep.2017.12.075

Martín-Rodríguez AJ, Villion K, Yilmaz-Turan S, Vilaplana F, Sjöling Å, Römling U (2021) Regulation of colony morphology and biofilm formation in *Shewanella algae*. Microb Biotechnol 14:1183–1200. https://doi.org/10.1111/1751-7915.13788

Masum MMI, Yang Y, Li B, Olaitan OS, Chen J, Zhang Y, Fang Y, Qiu W, Wang Y, Sun G (2017) Role of the genes of type VI secretion system in virulence of rice bacterial brown stripe pathogen Acidovorax *avenae* subsp. *avenae* strain RS-2. Int J Mol Sci 18:2024. https://doi.org/10.3390/ijms18102024

McCarter LL (2004) Dual flagellar systems enable motility under different circumstances. J Mol Microbiol Biotechnol 7:18–29. https://doi.org/10.1159/000077866

Ming L, Sheng C (2015) A novel adhesive factor contributing to the virulence of *Vibrio parahaemolyticus*. Sci Rep 5:14449. https://doi.org/10.1038/srep14449

Mizan MF, Jahid IK, Kim M, Lee KH, Kim TJ, Ha SD (2016) Variability in biofilm formation correlates with hydrophobicity and quorum sensing among *Vibrio parahaemolyticus* isolates from food contact surfaces and the distribution of the genes involved in biofilm formation. Biofouling 32:497–509. https://doi.org/10.1080/08927014.2016.1149571

Noh HJ, Nagami S, Kim MJ, Kim J, Lee NK, Lee KH, Park SJ (2015) Role of VcrD1 protein in expression and secretion of flagellar components in *Vibrio parahaemolyticus*. Arch Microbiol 197:397–410. https://doi.org/10.1007/s00203-014-1069-9

Osei-Adjei G, Gao H, Zhang Y, Zhang L, Yang W, Yang H, Yin Z, Huang X, Zhang Y, Zhou D (2017) Regulatory actions of ToxR and CalR on their own genes and type III secretion system 1 in *Vibrio parahaemolyticus*. Oncotarget 8(39):65809–65822. https://doi.org/10.18632/oncotarget.19498

Pan J, Zhao M, Huang Y, Li J, Liu X, Ren Z, Kan B, Liang W (2018) Integration host factor modulates the expression and function of T6SS2 in *Vibrio fluvialis*. Front Microbiol 9:962. https://doi.org/10.3389/fmicb.2018.00962

Qiao Y, Feng L, Jia R, Luo Y, Yang Q (2022) Motility, biofilm formation and associated gene expression in *Vibrio parahaemolyticus* impaired by co-culture with live *Ulva fasciata*. J Appl Microbiol 132:101–112. https://doi.org/10.1111/jam.15175

Reglinski M, Monlezun L, Coulthurst SJ (2023) The accessory protein TagV is required for full Type VI secretion system activity in *Serratia marcescens*. Mol Microbiol 119:326–339. https://doi.org/10.1111/mmi.15027

Reichow SL, Korotkov KV, Gonen M, Sun J, Delarosa JR, Hol WG, Gonen T (2011) The binding of cholera toxin to the periplasmic vestibule of the type II secretion channel. Channels (Austin) 5:215–218. https://doi.org/10.4161/chan.5.3.15268

Ronholm J, Petronella N, Chew Leung C, Pightling AW, Banerjee SK (2016) Genomic features of environmental and clinical *Vibrio parahaemolyticus* isolates lacking recognized virulence factors are dissimilar. Appl Environ Microbiol 82:1102–1113. https://doi.org/10.1128/AEM.03465-15

Salomon D, Gonzalez H, Updegraff BL, Orth K (2013) *Vibrio parahaemolyticus* type VI secretion system 1 is activated in marine conditions to target bacteria, and is differentially regulated from system 2. PLoS ONE 8:e61086. https://doi.org/10.1371/journal.pone.0061086

Salomon D, Klimko JA, Orth K (2014) H-NS regulates the *Vibrio parahaemolyticus* type VI secretion system 1. Microbiology (Reading) 160:1867–1873. https://doi.org/10.1099/mic.0.080028-0

Schmidt K, Santos-Matos G, Leopold-Messer S, El Chazli Y, Emery O, Steiner T, Piel J, Engel P (2023) Integration host factor regulates colonization factors in the bee gut symbiont *Frischella perrara*. Elife 12:e76182. https://doi.org/10.7554/eLife.76182

Shimohata T, Mawatari K, Iba H, Hamano M, Negoro S, Asada S, Aihara M, Hirata A, Su Z, Takahashi A (2012) VopB1 and VopD1 are essential for translocation of type III secretion system 1 effectors of *Vibrio parahaemolyticus*. Can J Microbiol 58:1002–1007. https://doi.org/10.1139/w2012-081

Silva AJ, Benitez JA (2016) *Vibrio cholerae* biofilms and cholera pathogenesis. PLoS Negl Trop Dis 10:e0004430. https://doi.org/10.1371/journal.pntd.0004330

Singh RP, Kumari K (2023) Bacterial type VI secretion system (T6SS): an evolved molecular weapon with diverse functionality. Biotechnol Lett 45:309–331. https://doi.org/10.1007/s10529-023-03354-2

Song H, Kang Y, Qian A, Shan X, Li Y, Zhang L, Zhang H, Sun W (2020) Inactivation of the T6SS inner membrane protein DotU results in severe attenuation and decreased pathogenicity of *Aeromonas veronii* TH0426. BMC Microbiol 20:1–11. https://doi.org/10.1186/s12866-020-01743-5

Soria-Bustos J, Ares MA, Gómez-Aldapa CA, González-Y-Merchand JA, Girón JA, De la Cruz MA (2020) Two type VI secretion systems of *Enterobacter cloacae* are required for bacterial competition, cell adherence, and intestinal colonization. Front Microbiol 11:560488. https://doi.org/10.3389/fmicb.2020.560488

Sun J, Li X, Qiu Y, Xue X, Zhang M, Yang W, Zhou D, Hu L, Lu R, Zhang Y (2022) Quorum sensing regulates transcription of the pilin gene mshA1 of MSHA pilus in *Vibrio parahaemolyticus*. Gene 807:145961. https://doi.org/10.1016/j.gene.2021.145961

Tchelet D, Keppel K, Bosis E, Salomon D (2023) *Vibrio parahaemolyticus* T6SS2 effector repertoires. Gut Microbes 15:2178795. https://doi.org/10.1080/19490976.2023.2178795

Wang L, Zhou D, Mao P, Zhang Y, Hou J, Hu Y, Li J, Hou S, Yang R, Wang R, Qiu J (2013) Cell density- and quorum sensing-dependent expression of type VI secretion system 2 in *Vibrio parahaemolyticus*. PLoS ONE 8:e73363. https://doi.org/10.1371/journal.pone.0073363

Wang SH, Dai JJ, Meng QM, Han XG, Han Y, Zhao YC, Yang DH, Ding C, Yu SQ (2014) DotU expression is highly induced during *in vivo* infection and responsible for virulence and Hcp1 secretion in avian pathogenic *Escherichia coli*. Front Microbiol 5:588. https://doi.org/10.3389/fmicb.2014.00588

Wang S, Liu X, Xu X, Yang D, Wang D, Han X, Shi Y, Tian M, Ding C, Peng D, Yu S (2016) *Escherichia coli* type III secretion system 2 ATPase EivC is involved in the motility and virulence of avian pathogenic *Escherichia coli*. Front Microbiol 7:1387. https://doi.org/10.3389/fmicb.2016.01387

Wang N, Liu J, Pang M, Wu Y, Awan F, Liles MR, Lu C, Liu Y (2018a) Diverse roles of Hcp family proteins in the environmental fitness and pathogenicity of *Aeromonas hydrophila* Chinese epidemic strain NJ-35. Appl Microbiol Biotechnol 102:7083–7095. https://doi.org/10.1007/s00253-018-9116-0

Wang X, Sun B, Xu M, Qiu S, Xu D, Ran T, He J, Wang W (2018b) Crystal structure of the periplasmic domain of TssL, a key membrane component of Type VI secretion system. Int J Biol Macromol 120:1474–1479. https://doi.org/10.1016/j.ijbiomac.2018.09.166

Wang S, Yan Q, Zhang M, Huang L, Mao L, Zhang M, Xu X, Chen L, Qin Y (2019) The role and mechanism of icmF in *Aeromonas hydrophila* survival in fish macrophages. J Fish Dis 42(6):895–904. https://doi.org/10.1111/jfd.12991

Wang X, Sun Y, Subedi D, Gong Q, Huang H, Li J, Wang Y, Ren J (2022) Hcp proteins of the type VI secretion system promote avian pathogenic *E. coli* DE205B (O2:K1) to induce meningitis in rats. Life 12:1353. https://doi.org/10.3390/life12091353

Wu Q, Li X, Zhang T, Zhang M, Xue X, Yang W, Hu L, Yin Z, Zhou D, Sun Y, Lu R, Zhang Y (2022) Transcriptomic analysis of *Vibrio parahaemolyticus* underlying the wrinkly and smooth phenotypes. Microbiol Spectr 10:e02188-e2222. https://doi.org/10.1128/spectrum.02188-22

Wu S, Tang J, Wang B, Cai J, Jian J (2023) Roles of Hcp2, a Hallmark of T6SS2 in Motility, Adhesive Capacity, and Pathogenicity of *Vibrio alginolyticus*. Microorganisms 11:2893. https://doi.org/10.3390/microorganisms11122893

Xiu P, Liu R, Zhang D, Sun C (2018) Bacterial aggregation assay in the presence of cyclic lipopeptides. Bio Protoc 8:e2686. https://doi.org/10.21769/BioProtoc.2686

Yang Z, Zhou X, Ma Y, Zhou M, Waldor MK, Zhang Y, Wang Q (2018) Serine/threonine kinase PpkA coordinates the interplay between T6SS2 activation and quorum sensing in the marine pathogen *Vibrio alginolyticus*. Environ Microbiol 20:903–919. https://doi.org/10.1111/1462-2920.14039

Yi L, Wang Y, Ma Z, Zhang H, Li Y, Zheng JX, Yang YC, Lu CP, Fan HJ (2013) Contribution of fibronectin-binding protein to pathogenesis of *Streptococcus equi* ssp. *zooepidemicus*. Pathog Dis 67:174–183. https://doi.org/10.1111/2049-632X.12029

Yu Y, Yang H, Li J, Zhang P, Wu B, Zhu B, Zhang Y, Fang W (2012) Putative type VI secretion systems of *Vibrio parahaemolyticus* contribute to adhesion to cultured cell monolayers. Arch Microbiol 194:827–835. https://doi.org/10.1007/s00203-012-0816-z

Yu Y, Fang L, Zhang Y, Sheng H, Fang W (2015) VgrG2 of type VI secretion system 2 of *Vibrio parahaemolyticus* induces autophagy in macrophages. Front Microbiol 6:168. https://doi.org/10.3389/fmicb.2015.00168

Zegadlo K, Gieron M, Zarnowiec P, Durlik-Popinska K, Krecisz B, Kaca W, Czerwonka G (2023) Bacterial motility and its role in skin and wound infections. Int J Mol Sci 24:1707. https://doi.org/10.3390/ijms24021707

Zhang L, Osei-Adjei G, Zhang Y, Gao H, Yang W, Zhou D, Huang X, Yang H, Zhang Y (2017a) CalR is required for the expression of T6SS2 and the adhesion of *Vibrio parahaemolyticus* to HeLa cells. Arch Microbiol 199:931–938. https://doi.org/10.1007/s00203-017-1361-6

Zhang YQ, Gao H, Osei-Adjei G, Zhang Y, Yang WH, Yang HY, Yin Z, Huang XX, Zhou DS (2017b) Transcriptional regulation of the type VI secretion system 1 genes by quorum sensing and ToxR in *Vibrio parahaemolyticus*. Front Microbiol 8:2005. https://doi.org/10.3389/fmicb.2017.02005

Zhang Y, Koehler AV, Wang T, Gasser RB (2020) *Enterocytozoon bieneusi* of animals-With an "Australian twist." Adv Parasitol 111:1–73. https://doi.org/10.1016/bs.apar.2020.10.001

Zhou D, Yan X, Qu F, Wang L, Zhang Y, Hou J, Hu Y, Li J, Xin S, Qiu J, Yang R, Mao P (2013a) Quorum sensing modulates transcription of cpsQ-mfpABC and mfpABC in *Vibrio parahaemolyticus*. Int J Food Microbiol 166:458–463. https://doi.org/10.1016/j.ijfoodmicro.2013.07.008

Zhou XH, Gewurz BE, Ritchie JM, Takasaki K, Greenfeld H, Kieff E, Davis BM, Waldor MK (2013b) A *Vibrio parahaemolyticus* T3SS effector mediates pathogenesis by independently enabling intestinal colonization and inhibiting TAK1 activation. Cell Rep 3:1690–1702. https://doi.org/10.1016/j.celrep.2013.03.039